Department of Physics and Astronomy

University of Heidelberg

Master thesis in Physics

submitted by

Rico Erhard

born in Oberkirch

2017

Transformed diffraction gratings, design and simulations

This Master thesis has been carried out by

Rico Erhard

at the

Chair of Optoelectronics

under the supervision of

Prof. Dr. Karl-Heinz Brenner

(Entwurf und Simulation transformierter Beugungsgitter):

Transformationsoptik ist eine Theorie, die auf der Forminvarianz der Maxwell-Gleichungen unter Koordinatentransformationen basiert. Unter Ausnutzung dieser Forminvarianz ist es möglich, Transformationen mit Änderungen in Materialien sowie mit transformierten elektromagnetischen Feldern zu verknüpfen. Mit dieser Verknüpfung lassen sich Medien entwerfen, welche die elektromagnetischen Felder gemäß der Entwurfstransformation transformieren. In dieser Arbeit wird diese Entwurfstechnik auf Beugungsgitter in einer Art und Weise angewendet, welche ihre Beugungseigenschaften unangetastet lässt. Die so entworfenen Medien werden mithilfe von Computersimulationen untersucht. Da diese Medien anisotrop und inhomogen sind, werden hierfür Methoden benötigt die auf solche Medien anwendbar sind. Der Gegenstand eines Teils dieser Arbeit sind solche Methoden. Sie werden im Hauptteil dazu verwendet, die Maxwell-Gleichungen in diesen Medien mit üblichen Randbedingungen zu lösen.

(Transformed diffraction gratings, design and simulations):

Transformation optics is a theory based on the formal invariance of Maxwell's equations under coordinate transformations. This formal invariance allows to relate transformations with changes in material parameters and with transformed electromagnetic fields. This relation can be exploited to design media that transform the electromagnetic fields according to the transformation used in the design. In this work, this design technique is used to transform diffraction gratings in a way that keeps their diffraction behaviour intact. The resulting transformation media are studied by means of computer simulations. Since these media are anisotropic and inhomogeneous, methods applicable to such media are needed to study them. One part of this work is devoted to such methods. These methods solve Maxwell's equations in the transformation media for usual boundary conditions in the main part of this work.

Contents

Chapter 1

Introduction

Transformation optics is a theory in the domain of classical electromagnetism. The theory is based on the formal invariance of Maxwell's equations under coordinate transformations [1, 2, 3, 4]. In his publication "Electromagnetic Waves in Gravitational fields" [1], published in 1960, Plebanski transformed the microscopic Maxwell equations in empty space to a curved geometry. Then he compares them with the macroscopic Maxwell equations in a space filled with matter. In doing so, he found constitutive equations for the electromagnetic fields. These constitutive equations contain transformation rules for the electric permittivity and the magnetic permeability that render the two sets of Maxwell equations equivalent. This can be understood as follows: The electromagnetic fields in the curved geometry behave exactly like fields in a flat geometry that is filled with a material described by constitutive equations. This is transformation optics in a nutshell.

A more thorough explanation is given in the section 2.1. An application of this theory, the main part of this work, is done in section 4. The transformation rules enable the design of media that transform the electromagnetic fields according to the transformation used in the design. This design technique is used to transform diffraction gratings in a way that keeps their diffraction behaviour intact. The transformed gratings as well as the original ones are studied by means of computer simulations and the results are compared to the theoretical predictions.

Since the transformed gratings are anisotropic and inhomogeneous, methods applicable to such media are needed to study them. Section 3 is devoted to such methods.

Chapter 2

Transformation optics

2.1 Plebanski's approach

In this section, a special case of Plebanski's constitutive equations is derived starting with Maxwell's equations and examples for constitutive equations.

The Maxwell equations are a set of partial differential equations that form the basis of classical electromagnetism. In macroscopic Minkowski form they read [5, section 2.1] [6, chapter 13]

$$\mathrm{rot}E = -\partial_t B, \tag{2.1a}$$
$$\mathrm{rot}H = J + \partial_t D, \tag{2.1b}$$
$$\mathrm{div}D = \rho, \tag{2.1c}$$
$$\mathrm{div}B = 0, \tag{2.1d}$$

with electric field strength E, magnetic field strength B, electric excitation D, magnetic excitation H, charge density ρ and current density J. The charge and current densities satisfy the continuity equation [7, §29] : $\mathrm{div}J + \partial_t \rho = 0$. If only the charge density is given and without additional information, the number of unknowns exceeds the number of equations in (2.1), hence additional information is needed to render the set of equations definite. This additional information is an interdependence between the electromagnetic field quantities E, B, D, H and J. The equations describing these interdependence are known as constitutive equations. And these constitutive equations incorporate the electromagnetic effects of the materials in the considered domain.

Electromagnetic effects in materials are very diverse [8] [9, section I.4] [5, section 2.2] and to my knowledge there is no consistent formulation of the constitutive equations that applies to all effects. Therefore, some common examples are given that apply to the physical problems treated in this work.

In linear isotropic materials such as glass, the fields are related by two scalars ε and μ [5, section 2.2.2]

$$D = \varepsilon E = \varepsilon_0 \varepsilon_r E, \tag{2.2a}$$
$$B = \mu H = \mu_0 \mu_r H, \tag{2.2b}$$

often expressed relative to the vacuum permittivity ε_0 and the vacuum permeability μ_0 [10, section 4.4.1]. This vacuum permittivity ε_0 is related to the vacuum permeability μ_0 and the speed of light c by [11, chapter 2]

$$c^2 = \frac{1}{\varepsilon_0 \mu_0}. \tag{2.3}$$

Assuming vacuum, $\varepsilon_r = \mu_r = 1$, the constitutive equations (2.2) can be used to substitute for D and H in equation (2.1) which yields

$$\mathrm{rot} E = -\partial_t B, \tag{2.4a}$$
$$\mathrm{rot} B = \mu_0 (J + \varepsilon_0 \partial_t E), \tag{2.4b}$$
$$\mathrm{div} E = \frac{\rho}{\varepsilon_0}, \tag{2.4c}$$
$$\mathrm{div} B = 0, \tag{2.4d}$$

the microscopic Maxwell equations. In linear anisotropic materials ε and μ are no longer scalars but matrices

$$D^i = \varepsilon^{ij} E_j, \tag{2.5a}$$
$$B^i = \mu^{ij} H_j. \tag{2.5b}$$

Note that Einsteins summation convention is used here. A prominent example for an anisotropic material is calcite. In this birefringent uniaxial crystal the constitutive equations (2.5) hold with the material parameters

$$\varepsilon_r = \begin{pmatrix} \sqrt{1.486} & 0 & 0 \\ 0 & \sqrt{1.685} & 0 \\ 0 & 0 & \sqrt{1.685} \end{pmatrix}, \quad \mu_r = \begin{pmatrix} 1 & 0 & 0 \\ 0 & 1 & 0 \\ 0 & 0 & 1 \end{pmatrix}, \tag{2.6}$$

for light with a wavelength around $0.590 \mu m$ in a suitable coordinate system whose axes coincide with the principal dielectric axes of the crystal [11, chapter 13] .

The preceding examples for constitutive equations are based on materials that exist in nature. The next example, Plebanski's constitutive equations [1], is not based on a existing material but on the form invariance of Maxwell's

equations. The derivation consists of two steps. The first step is to transform the microscopic Maxwell equations in empty space from a right handed Cartesian coordinate system to an arbitrary curvilinear coordinate system. The second step is to compare the resulting equations with Maxwell's equations in a macroscopic medium in a Cartesian coordinate system. Both sets are formally equivalent if the electromagnetic properties of this medium are described by Plebanski's constitutive equations [1, 12]

$$D^i = \varepsilon_0 \varepsilon_r^{ij} E_j + {}^{[ijk]} \frac{w_j}{c} H_k, \tag{2.7a}$$

$$B^i = \mu_0 \mu_r^{ij} H_j - {}^{[ijk]} \frac{w_j}{c} E_k, \tag{2.7b}$$

$$\varepsilon_r^{ij} = \mu_r^{ij} = -\frac{\sqrt{-g}}{g_{00}} g^{ij}, \quad w_i = \frac{g_{i0}}{g_{00}}, \tag{2.7c}$$

where ${}^{[ijk]}$ is the permutation symbol

$${}^{[ijk]} = \begin{cases} +1 & \text{if } (i,j,k) \text{ is } (1,2,3), (3,1,2), \text{ or } (2,3,1) \\ -1 & \text{if } (i,j,k) \text{ is } (1,3,2), (2,1,3), \text{ or } (3,2,1) \\ 0 & \text{if } i = j, \text{ or } j = k, \text{ or } k = i, \end{cases} \tag{2.8}$$

and g_{ij} is the metric tensor in the arbitrary coordinate system. The tensor g^{ij} is the inverse of the metric tensor g_{ij} [7, §83]:

$$g_{ik} g^{kj} = \delta_i^j, \tag{2.9}$$

where δ is the Kronecker delta. The metric tensor g_{ij} in the arbitrary coordinate system can be expressed as the transformation of the metric tensor η [7, §83]

$$g_{ij} = \Lambda^{i'}_{\ i} \Lambda^{j'}_{\ j} \eta_{i'j'}, \tag{2.10}$$

in another more familiar coordinate system. In Plebanski's paper [1] this is the metric of Minkowski space $\eta = \text{diag}\,(-1, 1, 1, 1)$ and Λ in equation (2.10) denotes the Jacobian matrix of the transformation

$$\Lambda^{i'}_{\ i} = \frac{\partial x^{i'}}{\partial x^i}, \tag{2.11}$$

from Minkowski space with coordinates x to the arbitrary coordinate system with coordinates x'. The g without indices in the expression $\sqrt{-g}$ is the determinant of the inverse of the metric tensor. This scalar can be expressed as the determinant of the Jacobi matrix and the determinant of the Minkowski

metric η which is -1. Taking the determinant on both sides of equation (2.10) gives

$$1/g = |\Lambda|^2|\eta| = -|\Lambda|^2 \Rightarrow \sqrt{-g} = \frac{1}{|\Lambda|}, \tag{2.12}$$

where the property of the determinant $|M^{-1}| = 1/|M|$ for a non-singular matrix M has been used. The material described by Plebanski's constitutive equations (2.7c) solely depends on the transformation used. The magnetic permeability of this material is equal to its electric permittivity and, if the vector w is non-zero, the material couples the electric fields with the magnetic fields. There is no guarantee that this material exists but if it is placed in empty space the empty space solution to Maxwell's equations become transformed versions of these empty space solutions.

Plebanski's derivation [1] is quite taciturn. A thorough derivation was published by Kulyabov and others [13], another one by Leonhardt and Philbin [12, appendix A] [2, appendix A] and yet another one by Ward and Pendry [14] but restricted to purely spatial transformations.

Plebanski's equations allow for transformations in space and time. Since only purely spatial transformations are used in this work and for the sake of simplicity a derivation for purely spatial transformations is presented.

In doing so, we transform Maxwell's equations (2.1) one after another from one reference frame to another keeping the time coordinate untouched. For this task, let f be a injective transformation from a Cartesian coordinate system x^1, x^2, x^3 to another x'^1, x'^2, x'^3,

$$x' = f(x), \tag{2.13}$$

with Jacobian matrix $\Lambda^{i'}_{\ i} = \frac{\partial x^{i'}}{\partial x^i}$.

In the Cartesian coordinate system the Maxwell equation (2.1a) in index notation reads

$$\mathcal{E}^{[ijk]}E_{k,j} = -\partial_t B^i, \tag{2.14}$$

in which the shortcut

$$V_{,j} = \frac{\partial V}{\partial x^j}, \tag{2.15}$$

is used. The symbol $\mathcal{E}^{[ijk]}$ is the Levi-Civita tensor. In equation (2.14) it is equal to $^{[ijk]}$ as defined in equation (2.8). This equality breaks when transforming to a different arbitrary coordinate system [7, §83] [2, sections 3.6, 3.9]:

$$\mathcal{E}^{[i'j'k']} = |\Lambda|\,{}^{[i'j'k']}. \tag{2.16}$$

This property comes into effect when we transform equation (2.14):

$$|\Lambda|\,{}^{[i'j'k']}E_{k',j'} = \mathcal{E}^{[i'j'k']}E_{k',j'} = -\partial_t B^{i'} \tag{2.17a}$$
$$= -\partial_t \Lambda^{i'}_{\ i} B^i \tag{2.17b}$$
$$= -\partial_t \Lambda^{i'}_{\ i} \mu^{ij} H_j \tag{2.17c}$$
$$= -\partial_t \Lambda^{i'}_{\ i} \mu^{im} \delta_m^{\ n} H_n \tag{2.17d}$$
$$= -\partial_t \Lambda^{i'}_{\ i} \mu^{im} \Lambda_m^{\ m'} \Lambda_{m'}^{\ n} H_n. \tag{2.17e}$$

Please note that $\Lambda_m^{\ m'}$ is the inverse of $\Lambda_{m'}^{\ n}$:

$$\Lambda_m^{\ m'} \Lambda_{m'}^{\ n} = \frac{\partial x^{m'}}{\partial x^m} \frac{\partial x^n}{\partial x^{m'}} = \delta_m^{\ n}, \tag{2.18}$$

and that contravariant vectors written with upper indices transform like

$$V^{i'} = \Lambda^{i'}_{\ i} V^i, \tag{2.19}$$

while covariant vectors transform like [7, §83]

$$V_{i'} = \Lambda^i_{\ i'} V_i. \tag{2.20}$$

Slightly rearranged, equation (2.17) becomes

$${}^{[i'j'k']}\left(\Lambda^{\ k}_{k'} E_k\right)_{,j'} = {}^{[i'j'k']}E_{k',j'} = -\partial_t \frac{\Lambda^{i'}_{\ i} B^i}{|\Lambda|} = -\partial_t \frac{\Lambda^{i'}_{\ i} \mu^{im} \Lambda_m^{\ m'}}{|\Lambda|} \Lambda_{m'}^{\ n} H_n. \tag{2.21}$$

With the definitions

$$\tilde{E} = \left(\Lambda^{-1}\right)^T E, \quad \tilde{B} = \frac{\Lambda B}{|\Lambda|}, \quad \tilde{\mu} = \frac{\Lambda \mu \Lambda^T}{|\Lambda|}, \quad \tilde{H} = \left(\Lambda^{-1}\right)^T H, \tag{2.22}$$

equation (2.21) can be written as

$$\mathrm{rot}\tilde{E} = -\partial_t \tilde{B} = -\partial_t \tilde{\mu} \tilde{H}, \tag{2.23}$$

that has the same form as its Cartesian counterpart (2.1a) with the same rotation operator as in Cartesian coordinates $(\mathrm{rot}V)^i := {}^{[ijk]}V_{j,k}$.

Repeating this procedure with the other rotation equation (2.1b) yields

$$|\Lambda|\,{}^{[i'j'k']}H_{k',j'} = \mathcal{E}^{[i'j'k']}H_{k',j'} = J^{i'} + \partial_t D^{i'} \tag{2.24a}$$
$$= \Lambda^{i'}_{\ i} J^i + \partial_t \Lambda^{i'}_{\ i} D^i \tag{2.24b}$$
$$= \Lambda^{i'}_{\ i} J^i + \partial_t \Lambda^{i'}_{\ i} \varepsilon^{ij} E_j \tag{2.24c}$$
$$= \Lambda^{i'}_{\ i} J^i + \partial_t \Lambda^{i'}_{\ i} \varepsilon^{im} \delta_m^{\ n} E_n \tag{2.24d}$$
$$= \Lambda^{i'}_{\ i} J^i + \partial_t \Lambda^{i'}_{\ i} \varepsilon^{im} \Lambda_m^{\ m'} \Lambda_{m'}^{\ n} E_n, \tag{2.24e}$$
$$\Rightarrow {}^{[i'j'k']}H_{k',j'} = \frac{\Lambda^{i'}_{\ i} J^i}{|\Lambda|} + \partial_t \frac{\Lambda^{i'}_{\ i} D^i}{|\Lambda|} = \frac{\Lambda^{i'}_{\ i} J^i}{|\Lambda|} + \partial_t \frac{\Lambda^{i'}_{\ i} \varepsilon^{im} \Lambda_m^{\ m'}}{|\Lambda|} \Lambda_{m'}^{\ n} E_n, \tag{2.24f}$$

and with the definitions

$$\tilde{J} = \frac{\Lambda J}{|\Lambda|}, \quad \tilde{D} = \frac{\Lambda D}{|\Lambda|}, \quad \tilde{\varepsilon} = \frac{\Lambda \varepsilon \Lambda^T}{|\Lambda|}, \tag{2.25}$$

equation (2.24) can be written as

$$\mathrm{rot}\tilde{H} = \tilde{J} + \partial_t \tilde{D} = \tilde{J} + \partial_t \tilde{\varepsilon}\tilde{E},$$

that is to say, in the same form as equation (2.1b).

It remains to be shown that the two remaining Maxwell equations (2.1c) and (2.1d) keep their form too. They contain divergences of vector fields that are not invariant under coordinate transformations [7, §86]:

$$(\mathrm{div}V)^{i'} = |\Lambda| \left(\frac{1}{|\Lambda|} V^{i'} \right)_{,i'}. \tag{2.26}$$

Using this property, we can rewrite (2.1c) in the primed coordinate system equation (2.17)

$$\frac{\rho}{|\Lambda|} = \left(\frac{1}{|\Lambda|} D^{i'} \right)_{,i'} = \left(\frac{1}{|\Lambda|} \Lambda^{i'}_{\ i} D^i \right)_{,i'} = \left(\frac{1}{|\Lambda|} \Lambda^{i'}_{\ i} \varepsilon^{ij} E_j \right)_{,i'} = \left(\frac{1}{|\Lambda|} \Lambda^{i'}_{\ i} \varepsilon^{im} \delta_m^{\ n} E_n \right)_{,i'} \tag{2.27a}$$

$$= \left(\frac{\Lambda^{i'}_{\ i} \varepsilon^{im} \Lambda_m^{\ m'}}{|\Lambda|} \Lambda^n_{\ m'} E_n \right)_{,i'}, \tag{2.27b}$$

or put differently

$$\mathrm{div}\left(\tilde{\varepsilon}\tilde{E}\right) = \mathrm{div}\tilde{D} = \tilde{\rho}. \tag{2.28}$$

in the form of (2.1c) with the new definition

$$\tilde{\rho} = \frac{\rho}{|\Lambda|}. \tag{2.29}$$

In the same way (2.1d) becomes

$$0 = \left(\frac{1}{|\Lambda|} B^{i'} \right)_{,i'} = \left(\frac{1}{|\Lambda|} \Lambda^{i'}_{\ i} B^i \right)_{,i'} = \left(\frac{1}{|\Lambda|} \Lambda^{i'}_{\ i} \mu^{ij} H_j \right)_{,i'} = \left(\frac{1}{|\Lambda|} \Lambda^{i'}_{\ i} \mu^{im} \delta_m^{\ n} H_n \right)_{,i'} \tag{2.30a}$$

$$= \left(\frac{\Lambda^{i'}_{\ i} \mu^{im} \Lambda_m^{\ m'}}{|\Lambda|} \Lambda^n_{\ m'} H_n \right)_{,i'}, \tag{2.30b}$$

and rewritten with the existing transformation rule (2.22) for μ

$$\operatorname{div}\left(\tilde{\mu}\tilde{H}\right) = \operatorname{div}\tilde{B} = 0, \tag{2.31}$$

this equation has the same form as equation (2.1d).

So, the transformed Maxwell's equations can be written in the same form as Maxwell's equations in a Cartesian coordinate system (2.23), (2.26), (2.28), (2.31), provided the following 'transformation rules' are used

$$\tilde{\varepsilon} = \frac{\Lambda\varepsilon\Lambda^T}{|\Lambda|}, \quad \tilde{\mu} = \frac{\Lambda\mu\Lambda^T}{|\Lambda|}, \tag{2.32a}$$

$$\tilde{J} = \frac{\Lambda J}{|\Lambda|}, \quad \tilde{\rho} = \frac{\rho}{|\Lambda|} \tag{2.32b}$$

$$\tilde{E} = \left(\Lambda^{-1}\right)^T E, \quad \tilde{D} = \frac{\Lambda D}{|\Lambda|} = \tilde{\varepsilon}\tilde{E}, \tag{2.32c}$$

$$\tilde{H} = \left(\Lambda^{-1}\right)^T H, \quad \tilde{B} = \frac{\Lambda B}{|\Lambda|} = \tilde{\mu}\tilde{H}. \tag{2.32d}$$

This means that, solving Maxwell's equations in the primed coordinate system is equivalent to solving them in a Cartesian system with changed permittivity $\tilde{\varepsilon}$, permeability $\tilde{\mu}$, charges and currents $\tilde{\rho}$, $\tilde{J}$.

In the following, the relation of the transformation rules (2.32a) to Plebanski's equations (2.7c) is given. The transformation rules (2.32a) also hold for relative permittivity $\tilde{\varepsilon_r} = \tilde{\varepsilon}/\varepsilon_0$ and relative permeability $\tilde{\mu_r} = \tilde{\mu}/\mu_0$ because ε_0 and μ_0 are just constant factors the equations (2.32a) can be divided with. For the choice $\varepsilon_r = \mu_r = 1$, that is, starting from vacuum:

$$\tilde{\varepsilon_r} = \tilde{\mu_r} = \frac{\Lambda 1 \Lambda^T}{|\Lambda|}. \tag{2.33}$$

In the three-dimensional Cartesian coordinate system the metric tensor and its inverse are the unit matrix. The inverse of the metric tensor in the primed system is $G^{-1} = \Lambda 1 \Lambda^T$ and the square root of its determinant is $\sqrt{|G^{-1}|} = \sqrt{g} = 1/|\Lambda|$ by analogy with equation (2.12). Inserting these into equation (2.33) yields

$$\tilde{\varepsilon_r} = \tilde{\mu_r} = \frac{\Lambda 1 \Lambda^T}{|\Lambda|} = \sqrt{g} G^{-1}, \tag{2.34}$$

from which the relation to Plebanski's equations (2.7c) is evident. The transformation rules (2.34) for ε and μ with initial vacuum are the three-dimensional version of Plebanski's constitutive equations.

2.2 Applications of transformation optics

The equivalence between transformations and changes in material parameters (2.32) can be used in several ways.

If one has a transformation from a vacuum space to a different space that corresponds to a given medium, the solution of Maxwell's equations in this medium is simply obtained by applying the transformation to the vacuum solution. So, instead of solving Maxwell's equations directly in the medium, one could try to find the corresponding transformation. But this is an inverse problem and not necessarily easier than solving Maxwell's equations directly. A solution for the desired medium might not even exist. For a simple medium where the electric permittivity is isotropic and $\tilde{\mu_r} = 1$ there is no corresponding transformation to the vacuum space. The reason can be seen in equation (2.33). Since both the electric permittivity and the magnetic permeability are changed in exactly the same manner we always get $\tilde{\varepsilon_r} = \tilde{\mu_r}$ transforming from vacuum. And this is different from the problem statement.

Of more practical use is the fact that electromagnetic problems in an arbitrary coordinate system can be calculated in a Cartesian system with adjusted material parameters [14]. A notable application of this technique is the C-Method [15, 16] where a transformation is chosen such that the grating surface of a one-dimensional relief grating becomes flat. This facilitates the treatment of the boundary conditions on the relief surface.

Another application is to use transformation optics as a design method [17]. In this technique one starts with a transformation one considers useful in some way and then, using the transformation rules (2.32), the material parameters follow directly. Provided one is able to fabricate these material parameters, one gets a device that applies the chosen design transformation to the fields travelling through it.

Perhaps the most prominent example of transformation optics design is the spherical or cylindrical cloaking device [18, 3] that guides the electromagnetic fields around a sphere rendering the objects inside invisible. This cloak is designed with a transformation that shifts the radial coordinate [18, 3]

$$r' = \begin{cases} \frac{R_2 - R_1}{R_2} r + R_1, & \text{if } 0 < r \leq R_2 \\ r, & \text{else,} \end{cases} \tag{2.35}$$

by the constant R_1, the radius of the cloaked sphere, and applies a stretching of the radial coordinate inside the cloak to achieve continuity at $r = R_2$, the outer radius of the cloak. A cylindrical and slightly modified version of this device that works almost as advertised for electromagnetic waves in a narrow

frequency band was realised by means of metamaterials [19]. These metamaterials consist of many sub-wavelength blocks that, when put together, act like a material with the desired material properties (ε, μ) not achievable with natural materials [20, 21, 22] [23, appendix C.1]. These blocks have to be smaller then the wavelength of the light the bulk device operates on [20]. This poses a substantial challenge to fabricate metamaterials for wavelengths in the visible band. The group around Schurig [19] built the cylindrical cloaking device with blocks smaller than a millimeter that operate on electromagnetic waves at around 8.5GHz.

More often than not the devices designed with transformation optics tend to require complicated materials. This includes anisotropic materials or materials with magnetic permeabilities different from unity that may be unavailable. But, in some designs it is possible to relax the material parameters a bit without completely losing the desired effect of the transformation medium [19, 24, 25]. For example, another group [26] devised a cloak for optical wavelengths with a relaxed parameter set including $\mu = 1$. They demonstrated numerically that the cloak still works with the relaxed material parameters, albeit not as perfectly as the original design.

2.3 Limitations of Plebanski's approach

The term that couples electric and magnetic fields in equation (2.7) through the vector w is only present if the transformation acts on time or depends on time. For purely spatial transformations without time dependence it is absent as in the equations (2.32). This magneto-electrical coupling term can be related to the velocity of the medium [2, sections 4.4, 5.4] [13, A. 3.].

But, according to Thompson, Cummer and Frauendiener [27, 28, 29] this interpretation can only be done if the medium is isotropic and moves slowly with respect to the speed of light. This group identifies the non-covariance of Plebanski's approach as a basic problem of the formalism presented in section 2.1. This non-covariance restricts Plebanski's constitutive equations (2.7c) to stationary media and slowly-moving isotropic media that have to be put into vacuum space-time. The same group [27, 28, 29] generalised Plebanski's approach and developed a covariant formalism for transformation optics that is valid for all transformations, general linear materials and arbitrary background space-times. One example where the results of the two formalisms differ is a time dependent spatial transformation $T(t, f(t)x, y, z)$ applied to a prior anisotropic medium with vanishing magnetoelectric coupling [29, section V].

Despite these limitations, I use the less general but much simpler theory

of section 2.1 which is valid with the restriction to purely spatial transformations that do not depend on time.

Chapter 3

Methods for the grating problem

3.1 The grating problem

This section defines the grating problem and describes methods to solve it. There is a bunch of methods for the grating problem and a neat overview has been written by Auer [23]. Most transformations inevitably introduce anisotropic permittivity and permeability tensors, hence the need to implement a method that can handle anisotropic media. The so-called differential method is applicable to anisotropic gratings [30, 31, 32, 33]. This method is used in chapter 4 in which transformations applied to gratings are studied by means of the numerical solution of Maxwell's equations.

In a Cartesian coordinate system depicted in figure 3.1 the grating is defined in the domain $h_0 \leq z < h$ surrounded by the two isotropic homogeneous domains $z < h_0$ and $h < z$. The grating is a periodic structure with respect to x, that may vary along the z-direction, but is invariant in the y-direction. In general, one could allow for periodicity in the y-direction as well. For the sake of simplicity, this work is restricted to one-dimensional gratings that are invariant in the y-direction. Besides, it is restricted to monochromatic electromagnetic fields that propagate in a direction perpendicular to the y-direction. The grating is defined by the electric permittivity and the magnetic permeability and free of any non-linear effects where the medium itself may depend on the electromagnetic fields or the intensity. Since the grating may

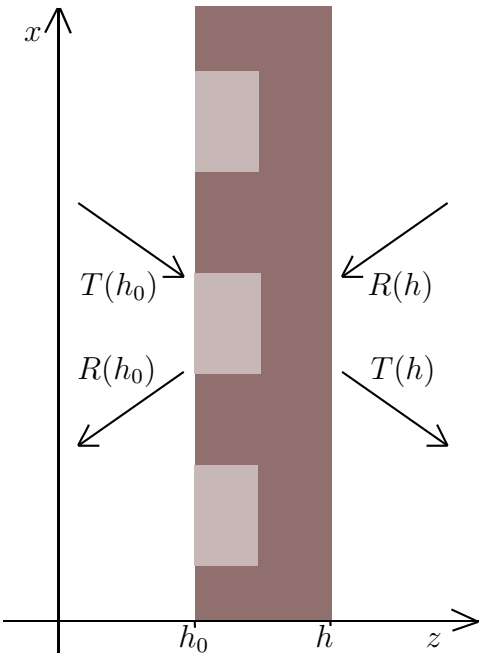

Figure 3.1: Schematic of a 1D-grating irradiated by plane waves with amplitudes $T(h_0), R(h)$ and diffracting plane waves with amplitudes $R(h_0), T(h)$.

be anisotropic, the permittivity and the permeability are matrices

$$\varepsilon(x,z) = \begin{pmatrix} \varepsilon_{xx}(x,z) & \varepsilon_{xy}(x,z) & \varepsilon_{xz}(x,z) \\ \varepsilon_{yx}(x,z) & \varepsilon_{yy}(x,z) & \varepsilon_{yz}(x,z) \\ \varepsilon_{zx}(x,z) & \varepsilon_{zy}(x,z) & \varepsilon_{zz}(x,z) \end{pmatrix},$$
$$\mu(x,z) = \begin{pmatrix} \mu_{xx}(x,z) & \mu_{xy}(x,z) & \mu_{xz}(x,z) \\ \mu_{yx}(x,z) & \mu_{yy}(x,z) & \mu_{yz}(x,z) \\ \mu_{zx}(x,z) & \mu_{zy}(x,z) & \mu_{zz}(x,z) \end{pmatrix}, \quad (3.1)$$

that are periodic with respect to x with a period p. It has been shown that the electromagnetic fields within the grating and beyond in such periodic problems are pseudo-periodic [34, 35, 5, 23, 32]. Pseudo-periodic means that the fields are periodic functions with a z-dependent phase and can be written as a pseudo-Fourier series. For instance, the x-component of the electric field

$$E_x(x,z) = \sum_{m=-\infty}^{\infty} E_{x,m}(z) \exp(ik_{x,m}x), \quad k_{x,m} = k_{x,0} + m\frac{2\pi}{p}, \quad (3.2)$$

where the time dependence $\exp(-i\omega t)$ is suppressed, p is the grating period and $k_{x,m}$ are the x-components of the wave vectors of each partial wave.

The constant $k_{x,0}$ allows to shift the center of $k_{x,m}$. For instance, $k_{x,0} = n_{\text{in}} k_0 \sin(\theta_{\text{in}})$ shifts the center to a value that corresponds to the x-component of the wave vector of a plane wave incident at an angle θ_{in} with vacuum wave number k_0 in an isotropic homogeneous region with refractive index n_{in}.

A short textual explanation for the pseudo-periodicity goes as follows. By definition, the grating is irradiated by waves of infinite extent with respect to x. In the grating the fields exist in a world that is periodic with respect to x and with period p. So, the fields in the grating must be periodic in the same sense, hence the fields diffracted off the grating must be periodic in the same sense. So, both the fields inside the grating as well as the fields in the two homogeneous isotropic domains must be periodic with respect to x and can be written as Fourier series like (3.2).

The two zones to the left ($z < h_0$) and to the right ($h \leq z$) of the grating are isotropic and homogeneous. In these homogeneous isotropic zones the electromagnetic fields can also be expanded with respect to z, known as Rayleigh expansion [34, section 1.2.3]

$$E_x(x,z) = \sum_{m=-\infty}^{\infty} \left(T_{xm}(z_0) e^{ik_{z,m}(z-z_0)} + R_{xm}(z_0) e^{-ik_{z,m}(z-z_0)} \right) e^{ik_{x,m}x}, \quad \text{(3.3a)}$$

$$k_{z,m} = \sqrt{k_0^2 \varepsilon_r \mu_r - k_{x,m}^2}, \quad k_0 = \frac{2\pi}{\lambda_0}, \quad \text{(3.3b)}$$

where light with vacuum wavelength λ_0 and a medium with refractive index $\sqrt{\varepsilon_r \mu_r}$ are assumed. The field E_x is expanded into an infinite number of plane waves described by wave vectors k with components k_x, k_z and $k_y = 0$. For each $k_{x,m}$ there are two plane waves with amplitudes $T_{x,m}$ and $R_{x,m}$, the latter propagating in the negative z-direction and the former propagating in the positive z-direction. The other components of the electric field can be expanded likewise but with the amplitudes $T_{x,m}$, $R_{x,m}$ exchanged by $T_{y,m}$, $R_{y,m}$ or $T_{z,m}, R_{z,m}$. But, $T_{x,m}$, $R_{x,m}$, $T_{y,m}$, $R_{y,m}$ alone form a basis for the electromagnetic fields in the isotropic homogeneous zones. The remaining amplitudes for the z-component of the electric field and for the magnetic field follow from Maxwell's equations.

Let $T(z)$ be a vector composed of $(T_x, T_y)^T$, where T_x and T_y are vectors composed of the amplitudes $T_{x,m}$ and $T_{y,m}$ and likewise for $R(z)$. Then $T(h_0)$ and $R(h)$ contain the amplitudes of all wave that move towards the grating while $R(h_0)$ and $T(h)$ do the same for waves that move away from the grating. The grating problem with so-called outgoing wave condition is defined is: Given $T(h_0)$ and $R(h) = 0$, what are $T(h)$ and $R(h_0)$? "Outgoing wave" because no light is coming from the right side. This is a special but quite usual boundary condition.

How electromagnetic fields propagate in the isotropic homogeneous regions is analytically known. But the propagation inside the grating structure is non-trivial. So, for solving this problem we need a method to propagate the fields through the grating and to achieve the desired boundary conditions on both sides of the grating.

3.2 The differential method

Maxwell's equations are a set of partial differential equations that govern the dynamics of electromagnetic waves. Partial differential equations are difficult to solve. What the differential method basically does is a translation of Maxwell's equations into a set of ordinary differential equations. Ordinary differential equations are very good understood and there are many numerical algorithms for their solution.

The differential method is a linear homogeneous ordinary differential equation derived from the Maxwell equations

$$\mathrm{rot}E = i\omega\mu H, \quad \mathrm{rot}H = -i\omega\varepsilon E, \tag{3.4}$$

in frequency space obtained by inserting pseudo Fourier series (3.2) for the electromagnetic fields into the Maxwell equations (2.1a), (2.1b). The z-components H_z and E_z of the electromagnetic fields can be eliminated and for the remaining field components an ordinary differential equation

$$\partial_z F(z) = iM(z)F(z), \quad F := \begin{pmatrix} [E_x] \\ [E_y] \\ [H_x] \\ [H_y] \end{pmatrix}, \tag{3.5}$$

can be derived that describes the propagation of the fields in the z-direction where M is a 4x4-block-matrix. The field vector F and the matrix M (for an inhomogeneous material) do depend on z but '(z)' is omitted here and there for the sake of brevity. The field vector is a stacking of four $(2N+1)$-column vectors. Each of these $(2N+1)$-column vectors contain the Fourier modes of the truncated pseudo Fourier series of the field components E_x, E_y, H_x, H_y. For example

$$[E_x] = \begin{pmatrix} E_{x(-N)} \\ E_{x(-N+1)} \\ \vdots \\ E_{x(N)} \end{pmatrix}, \tag{3.6}$$

is such a $(2N+1)$-column vector for the modes $E_{xm}(z)$ with $m \in [-N, \ldots, N]$ (see (3.2)). Since computer memory is limited the Fourier series have to be truncated at a certain truncation level N.

There are derivations for isotropic gratings [23, 36, 37] and for anisotropic gratings [30, 31, 32, 33]. The abstract form of the ordinary differential equation (3.5) holds for all of the cited derivations. But there are different ways to calculate the 4x4 block matrix M. For isotropic gratings two quarters of M are zero and the dimension of the ODE can be halved [23, 36, 37].

The differential equation (3.5) describes the evolution of the field vector through the grating. For a unique solution we need boundary conditions.

3.3 The boundary conditions

The differential equation (3.5) allows to numerically propagate the field vector through the grating structure. Knowing the field vector on one side of the grating, one could use one of the many integration algorithms for linear first-order ordinary differential equations to get the field vector at another position. In other words,

$$\partial_z F(z) = f(z, F(z)) = iM(z)F(z), \tag{3.7a}$$

$$F(h_0) = \Gamma_3, \tag{3.7b}$$

where Γ_3 is given. This is an initial value problem. But, the grating problem is not an initial value problem. It is a linear boundary value problem

$$\partial_z F(z) = f(z, F(z)) = iM(z)F(z), \tag{3.8a}$$

$$\Gamma_0 F(h_0) + \Gamma_1 F(h) - \Gamma_2 = 0, \tag{3.8b}$$

and has a boundary condition that depends on two positions, h_0 and h. The Γ_1, Γ_2 are $4(2N+1) \times 4(2N+1)$-matrices with rank $[\Gamma_1, \Gamma_2] = 4(2N+1)$ that set the boundary condition together with Γ_2. Note that the special case of either $\Gamma_0 = 0$ or $\Gamma_1 = 0$ is equivalent to an initial value problem.

The boundary conditions for the grating problem with outgoing-wave condition are described in terms of T and R (see section 3.1). This means the incident field on one side of the grating ($z < h_0$) is known and no light is incident from the other side ($h < z$). In terms of T and R this is

$$R(h) = 0, \tag{3.9a}$$

$$T(h_0) = L_{\text{in}}, \tag{3.9b}$$

where L_{in} stands for the desired spectrum of plane waves that irradiate the grating at $z = h_0$.

For some algorithms it is more convenient to use the boundary condition in terms of field vectors as in equation (3.8b). With the conversion matrix (A.1) that translates T and R to the field vector F it is possible to translate the boundary conditions back and forth. Doing this for the outgoing wave condition (3.9) using (A.24)

$$\begin{aligned} 0 &= \begin{pmatrix} 0 & 0 \\ 1 & 0 \end{pmatrix} \begin{pmatrix} T(h_0) \\ R(h_0) \end{pmatrix} + \begin{pmatrix} 0 & 1 \\ 0 & 0 \end{pmatrix} \begin{pmatrix} T(h) \\ R(h) \end{pmatrix} - \begin{pmatrix} 0 \\ L_{\text{in}} \end{pmatrix} \\ &= \begin{pmatrix} 0 & 0 \\ 1 & 0 \end{pmatrix} Q^{-1} F(0) + \begin{pmatrix} 0 & 1 \\ 0 & 0 \end{pmatrix} Q^{-1} F(h) - \begin{pmatrix} 0 \\ L_{\text{in}} \end{pmatrix}, \end{aligned} \tag{3.10}$$

yields

$$\Gamma_0 = \begin{pmatrix} 0 & 0 \\ 1 & 0 \end{pmatrix} Q^{-1}, \quad \Gamma_1 = \begin{pmatrix} 0 & 1 \\ 0 & 0 \end{pmatrix} Q^{-1}, \quad \Gamma_2 = \begin{pmatrix} L_{\text{in}} \\ 0 \end{pmatrix}, \tag{3.11}$$

by comparison of (3.8b) with (3.10). Now the boundary value problem for the grating problem with outgoing-wave condition in both formulations is complete. The next section is about the solution of these types of boundary value problems.

3.4 The solution of the grating problem

The solution of Maxwell's equations for the grating problem described in section 3.1 is equivalent to the solution of a two point boundary value problem (3.8b). The evolution of the field vector with respect to z is governed by a linear homogeneous ordinary differential equation with matrix M (3.5). For the outgoing wave condition the boundary conditions are fixed by equation (3.11). The only approximation so far is the truncation to $2N + 1$ modes of all Fourier expansions in the calculation. So, the solution of the Fourier truncated boundary value problem is expected to approach the exact solution of Maxwell's equations, the higher the truncation level N is chosen.

There are quite a few algorithms for solving two-point boundary value problems. For example, there are the shooting methods, finite difference schemes, the collocation method or the Ritz-Galerkin method [38, chapter 9] [39, chapter 18]. But before introducing specific algorithms for solving the grating problem in the sections 3.4.2 and 3.4.3, the next section treats two fundamental issues that concern all of them.

3.4.1 Memory and stiffness

This section is about two formidable challenges concerning all differential methods: memory consumption and stiffness. The memory consumption can

be estimated from the size of the matrix M in equation (3.5). The dimension of this quadratic matrix is $4(2N+1) \approx 8N$ for one-dimensional gratings. If every entry needs 16 bytes for saving both the real part and the complex part of the number in double precision, the amount of memory needed with the truncation level N is

$$\mathrm{mem}_{1\mathrm{D}}(N) = 16(8N)^2\mathrm{B} = 1024N^2\mathrm{B} = N^2\mathrm{KiB}. \tag{3.12}$$

Assuming a truncation level of $N = 100$, the memory requirement for M is about 10MiB which is not a big deal nowadays. For two-dimensional gratings, that is, if the y-direction is not invariant but is periodic too, the memory consumption for saving M grows with N^4

$$\mathrm{mem}_{2\mathrm{D}}(N) = 16(8N)^4\mathrm{B} = 64N^4\mathrm{KiB}, \tag{3.13}$$

if the same truncation level N is used in the two dimensions. For $N = 100$, this is about 6TiB, which is quite a lot nowadays. So, the memory consumption poses a big issue, in two-dimensional grating problems but not in one-dimensional ones.

Another formidable issue arises from the matrix M but this one is not restricted to 3D. Stiffness makes the numerical integration of ordinary differential equations more difficult [40, section 7.4]. If the eigenvalues of the matrix M are very different in magnitude, there are parts of the solution of the ordinary differential equation (3.5) that vary very slowly compared to other parts of the solution that vary rapidly even if the sum of all those parts is a smooth and slowly varying function [39]. Consequently, in order to have an accurate solution, explicit integrators have to take very small steps to keep track of the rapidly varying parts of the solution [39, 40].

It turns out that grating problems are stiff and that the stiffness grows with the truncation level [32, section 7.8]. But using a high truncation level N is desirable because N limits the accuracy of the differential method.

This is an intrinsic issue of the grating problem that most researchers in this field inevitably face [23, section 3.2] [41, 42, 31, 43, 44, 45, 46, 47, 37] and identify as pollution by evanescent modes. These evanescent modes are parts of the solution that grow or decay exponentially in the z-direction. Because computers have a limited machine precision, rounding errors may become too large and important digits may be lost in calculations. This results in numerical instabilities. The larger the domain of integration, the bigger the instabilities. Large can mean a grating thickness of $\lambda/2$ [34, chapter 4] depending on the truncation level and the material of the grating.

The stiffness due to the evanescent modes not only affects the stability of the numerical integration of the differential equation (3.5). As a consequence

it also affects the matching of the boundary conditions at the two boundaries. An explanation follows. All matching procedures turn the two point boundary value problem into algorithms involving initial value problems. In other words, at some stage in these algorithms a solution is propagated from one point to another, whether analytically or numerically. And if the solution of the initial value problem to be solved is ill-conditioned, the matching algorithm itself is ill-conditioned. And the propagation of the solution is ill-conditioned, since a slight change in the input may change drastically the output due to the exponentially varying parts of the solution, if they are present. And they are present if the truncation level N is sufficiently large [32, section 7.8].

Fortunately, there are countermeasures for the stiffness issue. There are numerous ways to improve the stability of the numerical integration for stiff initial value problems [40] [39, section 17.5] [48, chapter 5] . But this does not counter the ill-conditioned matching procedures due to evanescent modes explained in the previous paragraph. The evanescent modes can be avoided or decreased in number by decreasing the truncation level N or increasing the grating period p. Both of these countermeasures are undesirable. Changing the grating period changes the physical problem and decreasing the truncation level decreases the accuracy of the simulation. As mentioned in the previous paragraph, the problem becomes bigger, the larger the domain of integration, for the following reason: The blowup and the decay of the exponentially varying parts of the solution become more extreme, the larger the domain of integration. In that case, the matching between the boundaries of the domain of integration becomes unstable. If the domain of integration is small, the exponential blowup of the evanescent modes is lower and the matching procedure is better conditioned. Decreasing the grating thickness is undesirable because this changes the physical problem.

But even if the grating is homogeneous in the z direction, we have the freedom to view the whole grating domain $[h_0, h]$ as a stack of several fictitious subdomains $h_0 = z_0 < z_1 < ... < z_m = h$ with $m + 1$ subboundaries z_k. Each of the subdomains is much thinner than the whole domain. If the boundary value problem on the whole domain can be cast into an algorithm that consists of several initial value problems on the thin subdomains $[z_k, z_{k+1}]$, plus matching operations on neighbouring subboundaries, then, the single initial value problem over the whole domain with subsequent ill-conditioned matching over the whole domain at once is avoided.

This is the basic trick of the multiple shooting method [49], the enhanced transmittance matrix approach [37], the R-matrix propagation algorithm [50, 47] and the S-matrix propagation algorithm [46, 51, 52, 53, 45]. All of them solve the intrinsic stiffness issue of grating problems with this divide

and conquer strategy. They do this at the cost of additional computational complexity or memory consumption.

Studying these algorithms is not the aim of this work. But I think it is necessary to explain why they are needed and to explain the algorithms used for the research of transformed gratings treated in section 4 in order to enable reproducibility of the results.

3.4.2 The multiple shooting method

The shooting method reformulates the boundary value problem (3.8b) as a root finding problem involving an initial value problem [39, chapter 18] [38, chapter 9]. In the shooting method the solution at one boundary $F(h_0)$ is guessed initially [39, chapter 18] [38, chapter 9]. Using this guess of the solution at the boundary $z = h_0$, the solution $F(h)$ at the other boundary $z = h$ can be obtained by solving the initial value problem (3.7) along the interval $[h_0, h]$, in other words, by propagating the solution $F(h_0)$ from one boundary to the other. This can be done with numerical integrating methods for ordinary differential equations [40] [38, chapter 8] [54, chapter 9] [39, chapter 17] choosing an appropriate integrator and stepsize [40, section 7.4] since the ODE is stiff [section 3.4.1]. If the interval $[h_0, h]$ is homogeneous, the initial value problem (3.7) can be solved in one step

$$F(h) = V^{-1}\exp(iD(h - h_0))VF(h_0), \tag{3.14}$$

with a diagonalisation of the matrix $M = V^{-1}DV$ [40, section 1.3]. Having the solution candidates at both boundaries, $F(h_0), F(h)$, one can plug them into the boundary condition (3.8b) and evaluate whether the guess is good. The guess is perfect if the boundary condition (3.8b) is fulfilled, that is to say, if the residual

$$\Phi(F(h_0; \text{guess})) := \Gamma_0 F(h_0; \text{guess}) + \Gamma_1 F(h; \text{propagated guess}) - \Gamma_2, \tag{3.15}$$

of the boundary condition (3.8b) is zero in all entries. Let $\hat{T}(h_0 \mapsto h)$ be an operator that, when applied to a field vector, maps it from $z = h_0$ to $z = h$:

$$\hat{T}(h_0 \mapsto h)F(h_0) = F(h). \tag{3.16}$$

Then equation (3.15) can be written in a more intuitive form

$$\Phi(F(h_0)) := \left(\Gamma_1 + \Gamma_2\hat{T}(h_0 \mapsto h)\right) F(h_0) - \Gamma_3 \stackrel{!}{=} 0, \tag{3.17}$$

in which the general procedure of the shooting methods is evident. The problem of finding a solution of the boundary value problem (3.8b), that is, finding a solution to an ordinary differential equation that obeys boundary conditions at two points, is translated into the root finding problem $\Phi(F(h_0)) \stackrel{!}{=} 0$ which contains the initial value problem $\hat{T}(h_0 \mapsto h)F(h_0)$. Of course, the first guess for $F(h_0)$ seldom is perfect. But, there are methods, for example Newton's method, that enhance the guess iteratively [39, chapter 9] [54, chapter 4] [38, chapter 4] such that Φ approaches zero until a prescribed tolerance is achieved. The convergence to the solution is not guaranteed in all cases though. Good algorithms converge if the initial guess is close enough to the real solution and more often than not, the rate of convergence can be determined in advance [39, chapter 9]. Each new iteration of the shooting method involves finding a new guess (aiming) and propagating this guess (shooting), hence the name.

But whatever the root finding algorithm and whatever the integrator, this simple method suffers the stability problem explained in section 3.4.1. The residual Φ (3.17) is very sensitive to its input data $F(h_0)$ if evanescent modes are propagated over a distance large enough. This makes the root finding problem (3.17) ill-conditioned even in cases where the boundary value problem (3.8b) is well-conditioned [49].

The multiple shooting method cures this problem by a subdivision of the root finding problem (3.17) on the domain $[h_0, h]$ into a root finding problem on m subdomains $h_0 = z_0 < z_1 < \ldots < z_m = h$ for a solution that satisfies the same boundary conditions (3.17) at the two outermost boundaries ($z_0 = h_0$, $z_m = h$) and is continuous at the subboundaries $z_1, \ldots, z_{m-1}$. On each subdomain the solution is propagated over a distance $(z_{k+1} - z_k)$ much smaller than $(h - h_0)$:

$$F(z_{k+1}) = \hat{T}(z_k \mapsto z_{k+1})F(z_k) := \hat{T}_k F(z_k). \tag{3.18}$$

This subdivision increases the dimension of the root finding problem (3.8b)

$$\Phi = \begin{pmatrix} \Gamma_0 & 0 & \cdots & & & \Gamma_1\hat{T}_{m-1} \\ \hat{T}_0 & -1 & 0 & \cdots & & 0 \\ 0 & \hat{T}_1 & -1 & 0 & & \vdots \\ \vdots & & \ddots & \ddots & & \vdots \\ \vdots & & & \ddots & \ddots & 0 \\ 0 & & & 0 & \hat{T}_{m-2} & -1 \end{pmatrix} \begin{pmatrix} F(z_0) \\ F(z_1) \\ \vdots \\ \vdots \\ \vdots \\ F(z_{m-1}) \end{pmatrix} + \begin{pmatrix} \Gamma_2 \\ 0 \\ \vdots \\ \vdots \\ \vdots \\ 0 \end{pmatrix} \stackrel{!}{=} 0, \tag{3.19}$$

but decreases its sensitivity to the input data [49] [39, section 18.2] [38, chapter 9]. The first row of (3.19) is the residual of the boundary condition,

similar to equation (3.17). The other rows are the demand for continuity across the subboundaries. The shooting method with a single shooting interval (3.17) is a special case of this multiple shooting method (3.19) with the choice $m = 1$. For sufficiently many subdomains the stability problem due to the evanescent modes is evaded. But how many are needed depends on the total distance $(h - h_0)$, the truncation level N and the grating material (ε, μ).

Newton's method is not the only way to solve the problem (3.19). Maxwell's equations are linear and the response of the media in the domain of integration is assumed to be linear as well. With these restrictions there are linear maps that map the solution at one point $F(z)$ to the solution at another point $F(z + \Delta z)$ [35, sections 4.2 and 5.2] [34, chapter 4]. And linear maps in vector spaces of finite dimensions can be written as a matrix [55, section 2.2]. Therefore, it is possible to get matrix representations of the operators $\hat{T}$. With this knowledge, equation (3.19) can be viewed as linear system. And as a linear system it can be solved with numerical algorithms for linear systems, with direct algorithms [38, chapter 2], with iterative algorithms [38, chapter 11] and especially with algorithms that exploit the almost block diagonal form [56, 57] of equation (3.19).

The choice of the algorithm dictates whether transfer matrices are actually needed. But even if they are not needed, it can save computation time to calculate them once and use them many times. The solution of an initial value problem over a given interval is as simple as a matrix vector multiplication with the transfer matrix for that interval. Solving the same initial value problem numerically entails more computations. This last paragraph explains how to calculate transfer matrices. The transfer matrix for a homogeneous interval $[z_k, z_{k+1}]$ without modulation in the lateral direction is known analytically [58]. With modulation in the lateral direction, the diagonalisation technique in equation (3.14) can be used. But the intervals need not be homogeneous in the z-direction, the material may depend on z. In that most general case one can resort to the numerical method. The matrix representation of a linear map is determined by the images of the basis vectors [55, section 2.2]. These images are the solution of the initial value problems

$$\begin{aligned} \frac{\mathrm{d}}{\mathrm{d}z} F(z) = f(z, F(z)) = iM(z)F(z), \\ F(z_k) = e_i, \quad \text{for } i \in 0, \ldots, 4N, \end{aligned} \tag{3.20}$$

along the interval $[z_k, z_{k+1}]$ where e_i are vectors of a basis for the vector space $\mathbb{C}^{4(2N+1)}$ the field vector $F(z_k)$ lives in [34, section 4.2.2] [35, sections 4.2 and

5.2]. A popular choice is the following basis

$$\left\{ \begin{pmatrix} 1 \\ 0 \\ 0 \\ \vdots \end{pmatrix}, \begin{pmatrix} 0 \\ 1 \\ 0 \\ \vdots \end{pmatrix}, \begin{pmatrix} 0 \\ 0 \\ 1 \\ \vdots \end{pmatrix}, \dots \right\}, \tag{3.21}$$

consisting of $4\,(2N+1)$ vectors which is the dimension of the aforementioned vector space. These basis vectors are propagated numerically along the interval $[z_k, z_{k+1}]$ and the solutions at z_{k+1} are the images of the linear map and hence the columns of the transfer matrix $\hat{T}_k$ [34, section 4.2.2].

3.4.3 The S-matrix propagation algorithm

S-matrix is an abbreviation for scattering matrix. The scattering matrix $\check{S}$ [53, 52] relates the electric field amplitudes on both sides of the grating as follows

$$\begin{pmatrix} R(h_0) \\ T(h) \end{pmatrix} = \begin{pmatrix} \check{S}_{11} & \check{S}_{12} \\ \check{S}_{21} & \check{S}_{22} \end{pmatrix} \begin{pmatrix} T(h_0) \\ R(h) \end{pmatrix}. \tag{3.22}$$

The scattering matrix turns the boundary value problem (3.8b) into a matrix vector multiplication if the boundary conditions are chosen such that $T(h_0)$ and $R(h)$ are known while $R(h_0)$ and $T(h)$ are unknown. This section explains how to get $\check{S}_{11}$ and $\check{S}_{21}$. These two blocks are sufficient for the outgoing wave condition

$$\begin{pmatrix} R(h_0) \\ T(h) \end{pmatrix} = \begin{pmatrix} \check{S}_{11} \\ \check{S}_{21} \end{pmatrix} T(h_0), \tag{3.23}$$

where $T(h_0)$ is given and $R(h) = 0$.

In section 3.4.2 transfer matrices

$$F(z_k) = \hat{T}(z_{k+1} \mapsto z_k) F(z_{k+1}), \tag{3.24}$$

that relate the field vector at two different positions are used. Since the scattering matrix (3.23) is defined for amplitudes T, R, of Rayleigh expansions of the electric field (3.3), working with transfer matrices for these amplitudes is more convenient. With the conversion matrix Q (A.1) switching from one formulation to the other is not difficult:

$$\begin{pmatrix} T(z_k) \\ R(z_k) \end{pmatrix} = Q^{-1} \hat{T}(z_{k+1} \mapsto z_k) Q \begin{pmatrix} T(z_{k+1}) \\ R(z_{k+1}) \end{pmatrix} =: \check{T}(z_{k+1} \mapsto z_k) \begin{pmatrix} T(z_{k+1}) \\ R(z_{k+1}) \end{pmatrix}. \tag{3.25}$$

This basis change is not only possible in the isotropic homogeneous zones $z < h_0$, $h < z$. It is also valid at arbitrary positions inside the grating zone because adding infinitesimal vacuum layers at these positions does not change the grating physically but permits the use of Rayleigh expansions at these positions [53, 52].

Vincent [34, chapter 4] published a method in 1980 that uses a transmission matrix $\check{T}$ over the complete grating domain

$$\begin{pmatrix} T(h_0) \\ R(h_0) \end{pmatrix} = \begin{pmatrix} \check{T}_{11} & \check{T}_{12} \\ \check{T}_{21} & \check{T}_{22} \end{pmatrix} \begin{pmatrix} T(h) \\ R(h) \end{pmatrix}, \tag{3.26}$$

and is restricted the outgoing wave condition $R(h) = 0$. With this restriction a quick calculation reveals that

$$T(h) = \check{T}_{11}^{-1} T(h_0), \tag{3.27a}$$
$$R(h_0) = \check{T}_{21} T(h) = \check{T}_{21} \check{T}_{11}^{-1} T(h_0). \tag{3.27b}$$

Comparing this with equation (3.23) we can identify

$$\check{T}_{21} \check{T}_{11}^{-1} = \check{S}_{11}, \tag{3.28a}$$
$$\check{T}_{11}^{-1} = \check{S}_{21}, \tag{3.28b}$$

as the two blocks of the S-matrix. So, it seems as if this method solves all grating problems with outgoing wave condition by means of the two submatrices $\check{T}_{11}, \check{T}_{21}$ of the transfer matrix. And this is true, analytically. Numerically, it suffers the very same stability issues explained in section 3.4.1. Inevitably Vincent experienced this instability and found that the limits of applicability of this method are very sensitive to parameters such as the grating depth, the truncation level and the refractive index of the grating. Furthermore, he attributed the instability mainly to the matrix inversion [34, section 4.2.5]. This can be understood with the eigenvalues of the transfer matrix. The transfer matrix, representing a linear map for the solution across a given interval, reflects the exponential growth and decay of evanescent modes in its eigenvalues. Exponential growth results in a high amplification over large distances and hence in large eigenvalues. Exponential decay results in low eigenvalues. The condition number of a matrix A is defined as

$$\kappa(A) := ||A||\, ||A^{-1}|| \geq ||AA^{-1}|| = ||1|| = 1, \tag{3.29}$$

where $||\,.\,||$ is a matrix norm [38, section 2.2.2]. The condition number depends on the choice of the matrix norm. But whatever the choice of the norm, the condition number gives an estimate for the relative error for the

numerical solution of a linear system $Ax = b$ [38, section 2.2.2]. Since matrix inversion is done by the solution of $\dim(A)$ linear systems, the condition number can be used as an estimate for the numerical errors done in matrix inversion A^{-1} [59, section 1.2.7]. The spectral radius of the matrix gives a lower bound for compatible matrix norms [59, lemma 1.1.1]

$$\rho(A) \leq ||A||. \tag{3.30}$$

So, using that in equation (3.29) gives a lower bound

$$\kappa(A) = ||A||\ ||A^{-1}|| \geq \rho(A)\rho(A^{-1}), \tag{3.31}$$

for the condition number κ. If A has eigenvalues large in magnitude, its spectral radius $\rho(A)$ is large. If A has eigenvalues low in magnitude, the spectral radius of $\rho(A^{-1})$ is large because the inverse matrix A^{-1} has the inverse eigenvalues of A. The matrix to be inverted $\check{T}_{11}$ has both properties at the same time if exponentially growing and decaying parts of the solution are present and mapped by $\check{T}_{11}$ across a sufficiently large distance. Then, its condition number $\kappa(\check{T}_{11})$ is large and the inversion done in equation (3.27) is ill-conditioned.

Mapping across smaller distances keeps the exponential growth and decay within limits smaller than for larger distances. Then the condition numbers $\kappa(\check{T}_{11})$, $\kappa(\check{T}_{21})$, get lower and computations and inversions with these matrices get better conditioned. This is exploited by the divide and conquer technique used in the S-matrix propagation algorithm. Let us use a grid $h_0 = z_0 < z_1 < ... < z_m = h$ and the notation

$$T_k = T(z_k), \tag{3.32}$$
$$R_k = T(z_k), \tag{3.33}$$

for the amplitudes of the Rayleigh expansions at the two outermost boundaries z_0, z_m and at the infinitesimal vacuum layers located at the subboundaries. Furthermore, with m subdomains $[z_k, z_{k+1}]$ come m transfer matrices

$$\begin{pmatrix} T_k \\ R_k \end{pmatrix} = \begin{pmatrix} \check{T}_{k,11} & \check{T}_{k,12} \\ \check{T}_{k,21} & \check{T}_{k,22} \end{pmatrix} \begin{pmatrix} T_{k+1} \\ R_{k+1} \end{pmatrix}, \tag{3.34}$$

and the scattering matrix for the subdomain $[z_k, z_m]$ shall be defined as

$$\begin{pmatrix} R_k \\ T_m \end{pmatrix} = \begin{pmatrix} \check{S}_{k,11} \\ \check{S}_{k,21} \end{pmatrix} T_k. \tag{3.35}$$

Then inserting the first row of equation (3.34) into the first row of equation (3.35) yields

$$R_k = \check{S}_{k,11} T_k = \check{S}_{k,11} \left(\check{T}_{k,11} T_{k+1} + \check{T}_{k,12} R_{k+1} \right) \tag{3.36}$$

$$= \check{S}_{k,11} \left(\check{T}_{k,11} + \check{T}_{k,12} \check{S}_{k+1,11} \right) T_{k+1}, \tag{3.37}$$

while inserting the first row of equation (3.35) into the second row of equation (3.34) yields

$$R_k = \check{T}_{k,21} T_{k+1} + \check{T}_{k,22} R_{k+1} = \left(\check{T}_{k,21} + \check{T}_{k,22} \check{S}_{k+1,11} \right) T_{k+1}. \tag{3.38}$$

Combining both results gives the recursion

$$S_{k,11} = \left(\check{T}_{k,21} + \check{T}_{k,22} \check{S}_{k+1,11} \right) \left(\check{T}_{k,11} + \check{T}_{k,12} \check{S}_{k+1,11} \right)^{-1}. \tag{3.39}$$

Furthermore, inserting the first row of equation (3.34) into the second row of equation (3.35) yields

$$T_m = \check{S}_{k,21} T_k = \check{S}_{k,21} \left(\check{T}_{k,11} T_{k+1} + \check{T}_{k,12} R_{k+1} \right) \tag{3.40}$$

$$= \check{S}_{k,21} \left(\check{T}_{k,11} + \check{T}_{k,12} \check{S}_{k+1,11} \right) T_{k+1}. \tag{3.41}$$

Combining this with a shifted index version of itself

$$T_m = \check{S}_{k+1,21} T_{k+1}, \tag{3.42}$$

gives the recursion

$$\check{S}_{k,21} = \check{S}_{k+1,21} \left(\check{T}_{k,11} + \check{T}_{k,12} \check{S}_{k+1,11} \right)^{-1}. \tag{3.43}$$

Both equations (3.39) (3.43) give a recursion for calculating the scattering matrix blocks for the subdomain $[z_k, z_m]$ with the scattering matrix blocks for the subdomain $[z_{k+1}, z_m]$ and the transfer matrices for the subdomain $[z_k, z_{k+1}]$. Starting at $k = m$ and applying the recursion until $k = 0$ gives the scattering matrix blocks for the complete grating domain $[z_0, z_m]$. The recursion is started with $S_{m,11} = 0$ and $S_{m,21} = 1$. This corresponds to a layer with zero reflectance and a transmittance of 1 or, put differently, to the scattering matrix for an infinitesimal vacuum layer. In this calculation the scattering at the interfaces between the grating zone and the isotropic homogeneous zones is not yet taken into account. This means that without modification of these calculations, the grating is assumed to reside in vacuum. The additional scattering due to the presence of media around the grating can be incorporated before the recursion by setting different start values $S_{m,11}, S_{m,21}$ [52] or afterwards [53, section 4.3].

For the case of $m = 1$, the grid consists of two points $h_0 = z_0 < z_m = h$, hence no subdivision of the grating domain is done. In that case, the recursion equations (3.39), (3.43), are only called once and the result

$$\check{S}_{0,11} = \left(\check{T}_{1,21} + \check{T}_{1,22}\check{S}_{1,11}\right)\left(\check{T}_{1,11} + \check{T}_{1,12}\check{S}_{1,11}\right)^{-1} \overset{\check{S}_{1,11}=0}{=} \left(\check{T}_{1,21}\right)\left(\check{T}_{1,11}\right)^{-1}, \tag{3.44}$$

$$\check{S}_{0,21} = \check{S}_{0,21}\left(\check{T}_{0,11} + \check{T}_{0,12}\check{S}_{1,11}\right)^{-1} \overset{\check{S}_{1,11}=0}{=} \check{S}_{0,21}\left(\check{T}_{0,11}\right)^{-1} \overset{\check{S}_{1,21}=1}{=} \left(\check{T}_{0,11}\right)^{-1}, \tag{3.45}$$

is equivalent to Vincent's method (3.28). So, why and when is the recursive S-matrix algorithm more stable than Vincent's method? As explained earlier in this section the matrix of the transfer matrix $\check{T}_{11}$ used in Vincent's method (3.28) has a high condition number if exponentially growing and decaying parts of the solution are to be mapped across a sufficiently large distance $[h_0, h]$. This makes the inversion $\check{T}_{11}^{-1}$ ill-conditioned. In the S-matrix algorithm the matrices to be inverted are $\left(\check{T}_{k,11} + \check{T}_{k,12}\check{S}_{k+1,11}\right)$ in the recursion equation (3.39) and $\left(\check{T}_{k,11} + \check{T}_{k,12}\check{S}_{k+1,11}\right)$ in the recursion equation (3.43). These matrices contain transfer matrices too. But these transfer matrices map the solution from one subboundary to the next one, across a subdomain $[z_k, z_{k+1}]$, not across the whole grating domain. The more subdomains are used and the smaller the subdomains $[z_k, z_{k+1}]$, the lower are the condition numbers of these transfer matrices and their disastrous influence on the matrix inversion in the recursion formulas (3.39) (3.43) fades more and more away. The other matrix involved in the matrix inversions, $\check{S}_{k+1,11}$, relates the transmitted fields at the subboundary z_{m+1} with the transmitted fields at the same subboundary (3.35). This relation is no map across distances and hence no issues due to exponential growth and decay arise here. This is in contrast to the matrix $\check{S}_{k+1,21}$ that relates the transmitted fields at the subboundary z_{m+1} to the transmitted fields at the outermost boundary $z_m = h$. It is used in the recursion equation (3.43). But it is not involved in the matrix inversion.

Chapter 4

Transformed diffraction gratings

4.1 Axial linear transformations

In this section, a linear transformation in the z-direction is applied to a periodic medium within $-d < z < 0$. In a similar fashion the team around Roberts [60] transformed a planar-convex lens. The linear transformation leaves the lateral directions untouched, $x' = x$, $y' = y$, but transforms the axial directions as follows

$$z' = t(z) = \begin{cases} z + d(1-a), & \text{if } z < -d \\ az, & \text{if } -d \leq z < 0 \\ z, & \text{if } 0 \leq z, \end{cases} \tag{4.1}$$

with the inverse transformation

$$z = t^{-1}(z') = \begin{cases} z' - d(1-a), & \text{if } z' < -ad \\ z'/a, & \text{if } -ad \leq z' < 0 \\ z, & \text{if } 0 \leq z'. \end{cases} \tag{4.2}$$

The region $z < -d$ is shifted in order to make the transformation continuous at $z = -d$. This is the left boundary of the region $-d \leq z < 0$ and the transformation stretches or compresses this region by the factor $a \in \mathbb{R}$. Next to it, in the region $0 \leq z$, the transformation (4.1) is the identity. The material parameters of the transformed structure are calculated with the transformation rules (2.32)

$$\varepsilon' = \frac{\Lambda \varepsilon \Lambda^T}{|\Lambda|}, \quad \mu' = \frac{\Lambda \mu \Lambda^T}{|\Lambda|}, \tag{4.3}$$

where Λ is the Jacobian

$$\Lambda = \begin{pmatrix} 1 & 0 & 0 \\ 0 & 1 & 0 \\ 0 & 0 & \partial_z z' \end{pmatrix}, \tag{4.4}$$

and ε, μ are the permittivity and permeability of the original structure. If not otherwise mentioned, relative permittivity and permeability tensors are used throughout this section. Since the Jacobian is a matrix of derivatives, a constant shift yields a unit matrix as Jacobian with unit determinant. Thus, the contribution of the Jacobian matrix to μ' and ε' is a unit matrix in the regions $z < -d$ and $0 \leq z$. So,

$$\Lambda = \begin{cases} \begin{pmatrix} 1 & 0 & 0 \\ 0 & 1 & 0 \\ 0 & 0 & a \end{pmatrix}, & \text{if } -d \leq z < 0 \\ 1, & \text{else,} \end{cases} \tag{4.5}$$

and the determinant

$$|\Lambda| = \begin{cases} a, & \text{if } -d \leq z < 0 \\ 1, & \text{else.} \end{cases} \tag{4.6}$$

Inserting these results into (4.3) and assuming an isotropic ε yields

$$\tilde{\varepsilon} = \begin{cases} \begin{pmatrix} \frac{1}{a} & 0 & 0 \\ 0 & \frac{1}{a} & 0 \\ 0 & 0 & a \end{pmatrix} \varepsilon(x,z), & \text{if } -d \leq z < 0 \\ \varepsilon(x,z), & \text{else,} \end{cases} \tag{4.7}$$

and substituting z with the inverse transformation gives the relative permittivity of the transformation medium

$$\tilde{\varepsilon} = \begin{cases} \begin{pmatrix} \frac{1}{a} & 0 & 0 \\ 0 & \frac{1}{a} & 0 \\ 0 & 0 & a \end{pmatrix} \varepsilon(x, t^{-1}(z')), & \text{if } -d \leq t^{-1}(z') < 0 \\ \varepsilon(x, t^{-1}(z')), & \text{else.} \end{cases} \tag{4.8}$$

In the same way the relative permeability $\tilde{\mu}$ is

$$\tilde{\mu} = \begin{cases} \begin{pmatrix} \frac{1}{a} & 0 & 0 \\ 0 & \frac{1}{a} & 0 \\ 0 & 0 & a \end{pmatrix}, & \text{if } -d \leq t^{-1}(z') < 0 \\ 1, & \text{else,} \end{cases} \tag{4.9}$$

where $\mu = 1$ is assumed for the original medium. The transformation medium is given by the functional forms of $\tilde{\varepsilon}$ in equation (4.8) and $\tilde{\mu}$ in equation (4.8). Both are calculated with the transformation rules (2.32) derived in section 2.1. There, an interpretation is made. The Maxwell equations transformed to a primed coordinate system are considered as Maxwell's equations in the original Cartesian coordinate system with changed materials, charges, currents and fields. The numerical calculations done in this chapter are always done with both the original medium and the transformation medium. In both cases the numerical calculations are carried out in the same Cartesian coordinate system. The original medium is already defined in that system. The transformation medium in that system is given by the equations (4.8) (4.9) with the primes dropped.

An example follows. Let us consider a diffractive optical element (DOE) that consists of a phase plate of thickness $d < \lambda$ with varying refractive index in the x-direction. Since the plate is thin, the thin element approximation (TEA) can be used to describe its effect on a light wave u

$$u_+ = u_- \exp(i\hat{n}(x)k_0 d), \tag{4.10}$$

$$\hat{n}(x) = n(x) + i\kappa(x), \tag{4.11}$$

where $n(x)$ is the refractive index plate and κ is the extinction coefficient of the material [61, section 4.2]. This approximation is used to design a DOE that focuses a plane wave in the following way. A focus in position space is a δ-distribution and in frequency space it is a uniform distribution. A truncated discrete uniform distribution is set to zero for frequencies higher than NA/λ with respect to their absolute value. The result u_0 is propagated in vacuum in the negative z-direction over a distance f, the desired focal length. This is done by multiplying the discrete frequency distribution with the propagator

$$u(-f) = u_0 \exp(-i \operatorname{Re}(k_{z,m})\ f), \tag{4.12}$$

also known as angular spectrum method [61, section 3.3]. The $k_{z,m}$ used here are the same as in equation (3.3). Taking the real part of k_z does not change the result if $NA < 1$ but prevents numerical problems due to floating point arithmetic. Then, the wave $u(-f)$ is transformed back to position space. Then, the phase of this signal is binarised and translated to a refractive distribution $n(x)$ of thickness d with the thin element approximation (4.10). Within the limits of this approximation, this DOE produces a focus at $z = f$ when being illuminated by a plane wave with wavelength λ from the left. For the choice $\kappa = 0$, the DOE has no absorption.

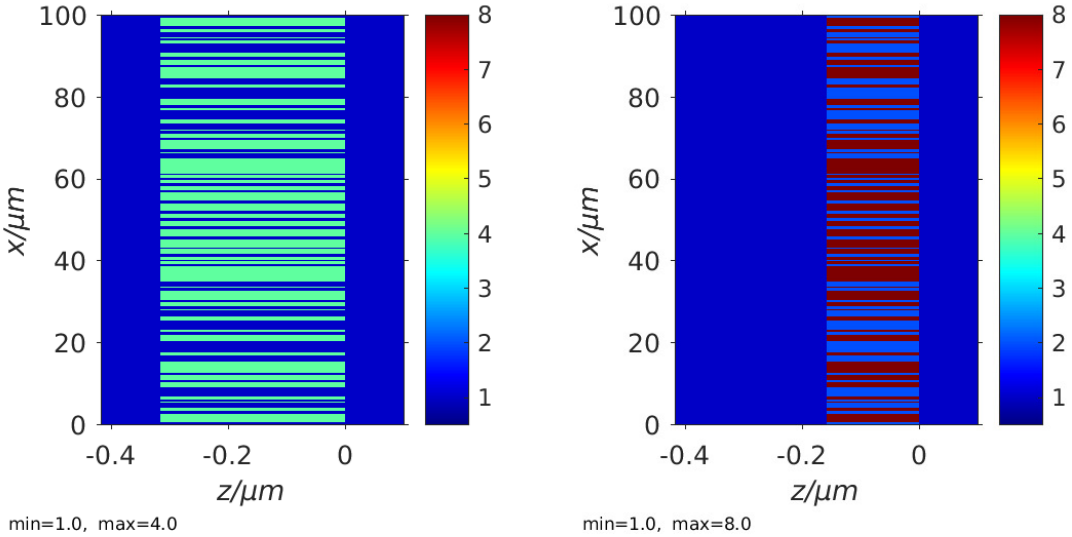

(a) original DOE, $\varepsilon_{xx} = \varepsilon_{yy} = \varepsilon_{zz}$ (b) $\tilde{\varepsilon}_{xx}$

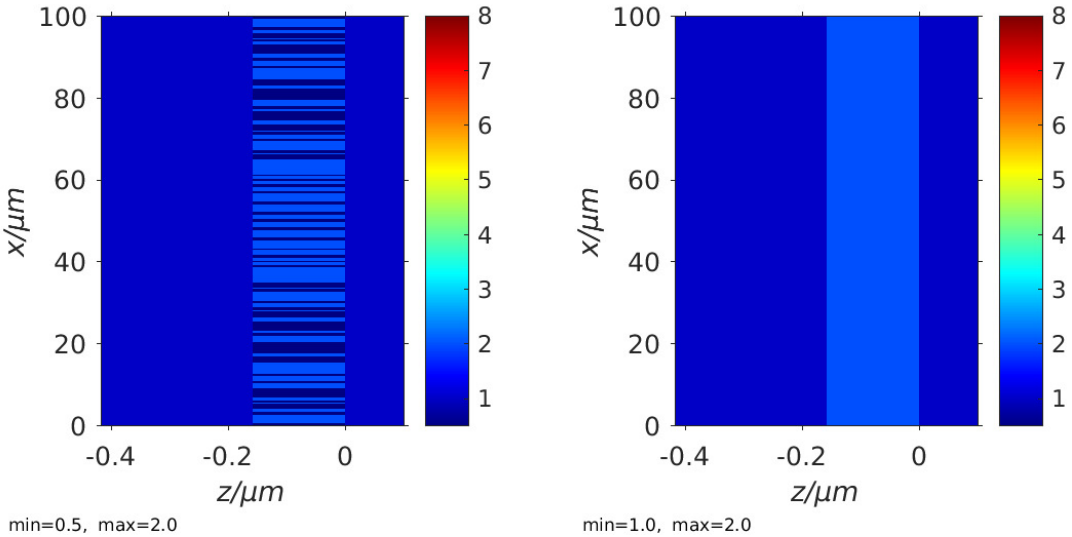

(c) $\tilde{\varepsilon}_{zz}$ (d) $\tilde{\mu}_{xx}$

Figure 4.1: Relative permittivity of the original DOE 4.1(a) and several components of the relative permittivity and permeability tensors of the transformed DOE. The latter, $\tilde{\varepsilon}$ and $\tilde{\mu}$, are determined by the equations (4.8), (4.9).

For the choices $\lambda = 0.633\mu m$, thickness $d = \lambda/2$, $f = 1000\mu m$, $NA = 0.5$, period $p = 100\mu m$, and two states for the refractive index, one of them unity, the corresponding relative permittivity $\varepsilon_{xx} = \sqrt{n}$ is shown in figure 4.1(a).

The relative permittivity and permeability tensors of the transformed version of this device are determined by the equations (4.8), (4.9) and some components are depicted in figure 4.1 for the choice $a = 1/2$. This choice makes the transformed plate half as thick as the original plate.

Since the transformation leaves the region $0 < z$ unchanged and is continuous everywhere else, I expect the transmitted light in this region to be the same for both devices if both of them are irradiated with the same light from the left. To check this, I solve Maxwell's equations numerically for both problems as a one-dimensional grating problem (section 3.1) with outgoing wave boundary condition (section 3.3) by means of the differential method (section 3.2) in combination with the multiple shooting method (section 3.4.2). This implies assuming periodicity in the x-direction.

On the left boundary, a perpendicularly incident plane wave of amplitude $1V/m$ linearly polarised in the y-direction is chosen as boundary condition. In terms of amplitudes R and T of plane waves used in Rayleigh expansions of the electrical field (3.3) (A.3) the boundary conditions are

$$R(0) = 0, \tag{4.13}$$

$$T_{xm}(h_0) = 0, \quad \forall\, m \in \{-N, \ldots, N\}\,, \tag{4.14}$$

$$T_{ym}(h_0) = \begin{cases} 1, & \text{if } m = 0 \\ 0, & \text{else,} \end{cases} \tag{4.15}$$

and $k_{x,0} = 0$, where h_0 is $-d$ for the original DOE and $-d/2$ for the transformed DOE.

For the differential method, I calculate the matrix M of the differential equation (3.5) in the way described by Watanabe, Petit and Nevière in 2002 [30, equation 65], but with three modifications. One is a different naming of the coordinate axes: my z-axis is their inverted y-axis. The second modification is the choice $\varphi = 0$ throughout all calculations. The differential method in this paper can be used for relief gratings with a surface function whose derivative is $\tan(\varphi)$. I treat the DOE as a stack of many planar ($\varphi = 0$) grating layers. The third modification affects the equations 45-52 in the same paper [30] and concerns the discrete convolutions in truncated frequency space. The discrete convolutions in these equations are written as a matrix vector where the matrix is a Toeplitz matrix built from one of these vectors. Due to Auer's findings [36, section 3.5] [62] and advice from my colleagues, I decided to use circulant Toeplitz matrices in these equations.

To solve the boundary value problems, I apply the multiple shooting described in section 3.4.2 with eight equally spaced subdomains and a truncation level of $N = 333$. I obtain the Fourier coefficients of the material functions by evaluating them on a grid of 2N + 1 equidistant points over one period and subsequent application of discrete Fourier transformations on the results. I calculate the transfer matrix for the subdomains with the diagonalisation technique (3.14) and solved the linear system (3.19) with the matlab [63] routine "mldivide". Furthermore, I use the matlab routines "fft" for discrete Fourier transforms, "inv" for Matrix inversions and "eig" for diagonalisations. For the design of the original DOE I use a matlab script once written by Tim Stenau with minor modifications.

The transmitted fields in the region $0 < z$ should be identical in both cases. The solution of the linear system contains $F(z_0), \ldots (z_{m-1})$. So, to get the solution at the right boundary $z = 0$ one last multiplication with a transfer matrix $F(0) = F(z_m) = T_{m-1}F(z_{m-1})$ is necessary. With the solution at the right boundary $F(0)$ for both problems, I calculate the propagative fields in the region $0 < z$ by means of the Rayleigh expansion (A.3). With these results, the two plots shown in figure 4.2 were created. There is no discernible difference for the naked eye between both plots. But a small difference can be seen in the numbers

$$\left\| F(0) - \tilde{F}(0) \right\|_1 = \sum_m \left| F_m(0) - \tilde{F}_m(0) \right| \approx 1.6\ 10^{-11}, \tag{4.16}$$

that I attribute to numerical errors in either the solution of the linear system (3.19) or the diagonalisation (3.14).

The question arised whether this works also with non-perpendicular incidence. So, I repeated the same calculations with slightly different boundary conditions at the left boundary

$$T_{ym}(h_0) = \begin{cases} 1, & \text{if } m = 1 \\ 0, & \text{else.} \end{cases} \tag{4.17}$$

This corresponds to a plane wave with an incident angle of about 0.36°. As depicted in figure 4.3 the foci are shifted and their shape has changed. But again, there is no discernible difference for the original and the transformed DOE. And the ℓ_1 norm of the difference of the solutions at the right boundary does not change much

$$\left\| F(0) - \tilde{F}(0) \right\|_1 \approx 1.3\ 10^{-11}. \tag{4.18}$$

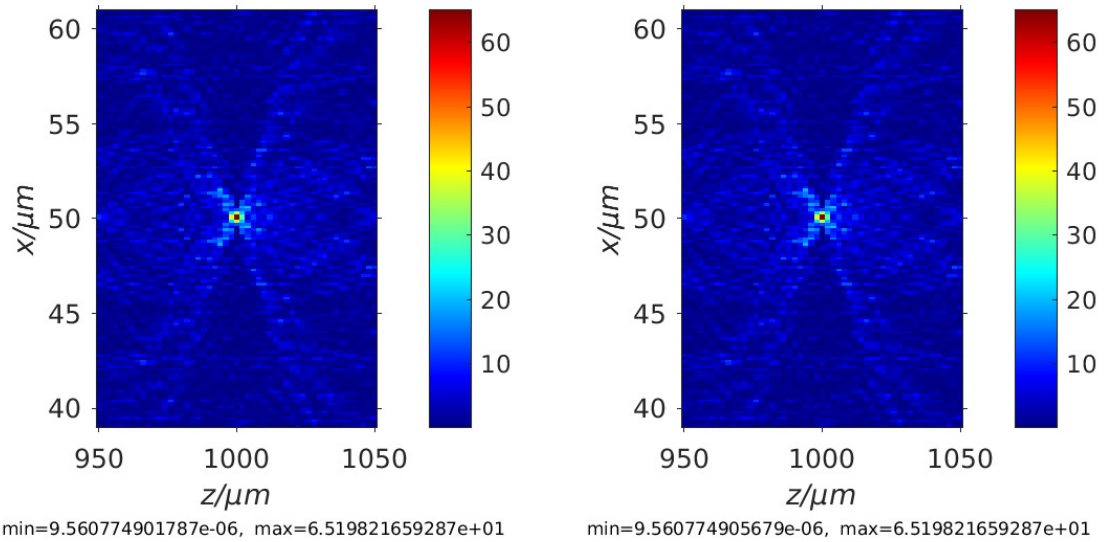

(a) focus of the original DOE (b) focus of the transformed DOE

Figure 4.2: Comparison of the foci of the original and the transformed DOE being irradiated perpendicularly by a plane wave. The plots show $|E|^2/(V/m)^2$ in a region around the expected focal point.

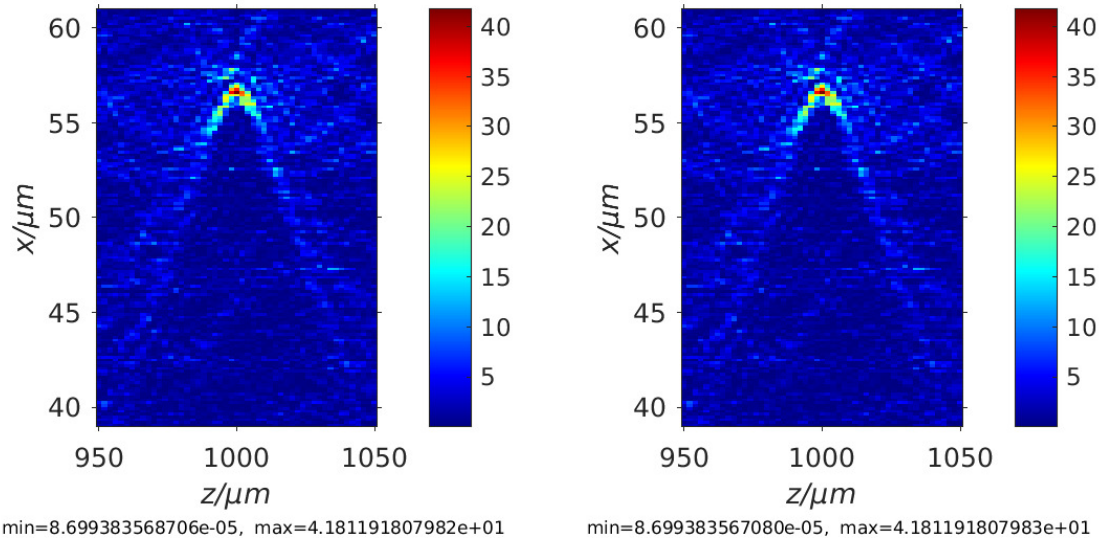

(a) focus of the original DOE (b) focus of the transformed DOE

Figure 4.3: Comparison of the foci of the original and the transformed DOE being irradiated by a plane wave with an angle of incidence of about 0.36°. The plots show $|E|^2/(V/m)^2$ in a region around the expected focal point.

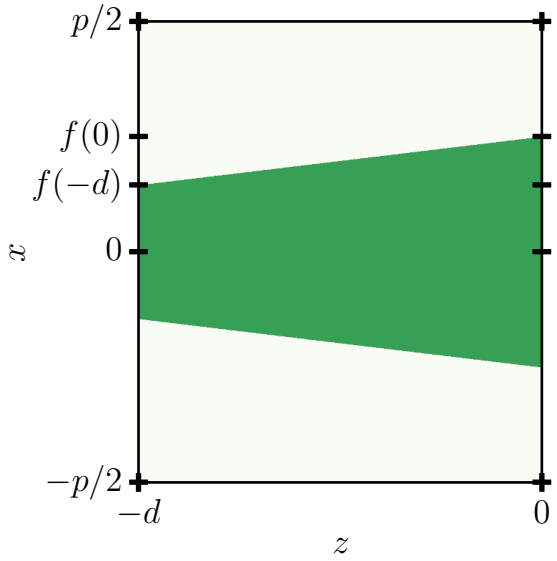

Figure 4.4: Relative permittivity distribution (4.19) of a grating with a linear contour $f(z)$.

4.2 Lateral cubic transformations

In this section, a cubic transformation in the x-direction is applied to gratings with the aim to keep their diffraction efficiencies unchanged. If not otherwise mentioned, relative permittivity and permeability tensors are used throughout this section. The relative permittivity function of the original grating shall be defined as

$$\varepsilon(x,z) = \begin{cases} \varepsilon_1, & \text{if } |x| < f(z) \text{ and } -d \le z \le 0 \\ \varepsilon_2, & \text{if } f(z) \le |x| \text{ and } -d \le z \le 0 \\ 1, & \text{else,} \end{cases} \tag{4.19}$$

in a period $x \in [-p/2, p/2]$ with a continuous function $f(z)$ that defines the lateral contour of the grating. A schematic example for a linear contour $f(z)$ is depicted in figure 4.4. The relative permeability of the original grating shall be one.

In the last section a linear contraction in the z-axis is done. Here, I present you a transformation that maps the contour $f(z)$ of the aforementioned grating to a constant. Therefore a transformation in the x-direction is needed. I demand the transformation to be continuous everywhere because additional reflections occur at discontinuities [64, 65]. These additional reflections have an impact on the diffraction efficiencies I want to preserve.

Furthermore, the transformation shall preserve the axial symmetry of the problem (4.19). This is not a necessity but shortens the calculations.

Let $t(x, z)$ denote the transformation. Then the properties

$$t(x, z) = -t(-x, z) \tag{4.20a}$$

$$t\left(\frac{p}{2}, z\right) = \frac{p}{2} \tag{4.20b}$$

$$t(f(z)) = x_c, \tag{4.20c}$$

ensure that the transformation preserves the axial symmetry of the problem (4.20a), is continuous at the period boundaries (4.20b) and maps the contour f to the constant x_c (4.20c). The transformation t defined by these properties (4.20) is applied locally on a finite domain $[z_{\min}, z_{\max}]$ that contains the domain of the original grating $(-d, 0] \subseteq [z_{\min}, z_{\max}]$. Outside of $[z_{\min}, z_{\max}]$ the transformation is the identity by definition. At the boundaries of this non-trivially transformed domain the transformation has to be continuous as well. This implies

$$t(x, z) = x, \quad \text{if } z \leq z_{\min} \text{ or } z_{\max} \leq z. \tag{4.21}$$

Since the inverse transformation is needed for the material of the transformed grating, the last property imposed on the transformation is injectivity.

A cubic polynomial

$$t(x, z) = a_0(z) + a_1(z)x + a_2(z)x^2 + a_3(z)x^3, \tag{4.22}$$

has enough degrees of freedom to satisfy all desired properties (4.20) and may be injective. From property (4.20a) follows $a_0(z) = 0 = a_2(z)$, so

$$t(x, z) = a_1(z)x + a_3(z)x^3. \tag{4.23}$$

Then from property (4.20b)

$$\frac{p}{2} = t\left(\frac{p}{2}, z\right) = a_1(z)\frac{p}{2} + a_3(z)\left(\frac{p}{2}\right)^3 \Rightarrow a_1(z) = 1 - a_3(z)\left(\frac{p}{2}\right)^2, \tag{4.24}$$

and with property (4.20c)

$$\begin{aligned} x_c = t(f(z), z) &= a_1(z)f(z) + a_3(z)f^3(z) \\ &\overset{(4.24)}{=} \left(1 - a_3(z)\left(\frac{p}{2}\right)^2\right) f(z) + a_3(z)f^3(z) \\ &= a_3(z)\left(f^3(z) - f(z)\left(\frac{p}{2}\right)^2\right) + f(z), \end{aligned} \tag{4.25}$$

follows

$$a_3(z) = \frac{x_c - f(z)}{f^3(z) - f(z)\left(\frac{p}{2}\right)^2} = \frac{1 - x_c/f(z)}{\left(\frac{p}{2}\right)^2 - f^2(z)}. \tag{4.26}$$

With these coefficients, the properties (4.20) are satisfied. If $f(x,z)$ grows strictly monotonically with respect to x, it is injective:

$$\begin{aligned} 0 < \partial_x f(x,z) &= a_1(z) + 3a_3(z)x^2 \\ &= 1 - \frac{p}{2}a_3(z) + 3a_3(z)x^2 = 1 - a_3(z)\left(\left(\frac{p}{2}\right)^2 + x^2\right), \end{aligned} \tag{4.27}$$

if $a_3(z) \leq 0$ this is true. If $0 < a_3(z)$

$$\begin{aligned} &0 < 1 - a_3(z)\left(\left(\frac{p}{2}\right)^2 + 0\right) \leq 1 - a_3(z)\left(\left(\frac{p}{2}\right)^2 + x^2\right) = \partial_x f(x,z) \\ &\Rightarrow a_3(z)\left(\frac{p}{2}\right)^2 < 1 \overset{(4.26)}{\Rightarrow} \left(\frac{p}{2}\right)^2 \frac{1 - x_c/f(z)}{\left(\frac{p}{2}\right)^2 - f^2(z)} < 1 \Rightarrow 1 - \frac{x_c}{f(z)} < 1 - \frac{f^2(z)}{\left(\frac{p}{2}\right)^2} \\ &\Rightarrow \frac{x_c}{f(z)} < \frac{f^2(z)}{\left(\frac{p}{2}\right)^2} \Rightarrow f(z) < \sqrt[3]{x_c\left(\frac{p}{2}\right)^2} =: f_{\max}. \end{aligned} \tag{4.28}$$

So, for the transformation to be injective the contour $f(z)$ must not exceed the threshold $f_{\max}$ which depends on the grating period and x_c.

There is an analytical expression for the inverse transformation. It is $t^{-1}(x') = x/a_1$, if $a_3 = 0$. If $a_3 \neq 0$, the analytical expression is complicated. It contains divisions by a_3 which approaches zero as f approaches x_c. Therefore, I avoid to evaluate this expression. Instead, I use a simpler way to invert the transformation. I solve $t(x) - x' = 0$ for x iteratively by means of Newton's method [54, section 18.1].

With the coefficients of the transformation (4.22) and its inverse, the relative permittivity and permeability distributions of the transformed grating can be calculated with the transformation rules (2.32). The Jacobian matrix of the transformation (4.23) reads

$$\Lambda = \begin{pmatrix} \partial_x t(x,z) & 0 & \partial_z t(x,z) \\ 0 & 1 & 0 \\ 0 & 0 & 1 \end{pmatrix} = \begin{pmatrix} a_1 + 3a_3x^3 & 0 & (\partial_z a_1)x + (\partial_z a_3)x^3 \\ 0 & 1 & 0 \\ 0 & 0 & 1 \end{pmatrix}, \tag{4.29}$$

thus the transformed relative magnetic permeability is

$$\tilde{\mu}(x',z) = \frac{\Lambda 1 \Lambda^T}{|\Lambda|} = \begin{pmatrix} \tilde{\mu}_{xx} & 0 & \tilde{\mu}_{xz} \\ 0 & \tilde{\mu}_{yy} & 0 \\ \tilde{\mu}_{xz} & 0 & \tilde{\mu}_{yy} \end{pmatrix}, \tag{4.30}$$

with

$$\tilde{\mu}_{yy} = \left(3x^2 a_3(z) + a_1(z)\right)^{-1} = \left(3\left(t^{-1}(x',z)\right)^2 a_3(z) + a_1(z)\right)^{-1}, \tag{4.31}$$

$$\tilde{\mu}_{xz} = \left(x^3 \partial_z a_3(z) + x\partial_z a_1 z)\right)\tilde{\mu}_{yy} \tag{4.32}$$

$$= \left(\left(t^{-1}(x',z)\right)^3 \partial_z a_3(z) + t^{-1}(x',z)\partial_z a_1(z)\right)\tilde{\mu}_{yy}, \tag{4.33}$$

$$\tilde{\mu}_{xx} = \left(1 + \tilde{\mu}_{xz}^2\right)/\tilde{\mu}_{yy}, \tag{4.34}$$

and the transformed relative electric permittivity can be written as

$$\tilde{\varepsilon}(x',z) = \frac{\Lambda\varepsilon\Lambda^T}{|\Lambda|} = \varepsilon\frac{\Lambda 1\Lambda^T}{|\Lambda|} = \varepsilon(t^{-1}(x',z),z)\,\tilde{\mu}(x',z). \tag{4.35}$$

An example follows.

4.2.1 Straightening of a linear contour

In this section, the cubic transformation (4.23) is applied to a grating as defined in equation (4.19) with $\varepsilon_1 = 2$, $\varepsilon_2 = 1$, period $p = 1\mu m$, thickness $d = 1\mu m$ and the linear contour

$$f(z) = p/4 - \tan(1^\circ)\,|z|. \tag{4.36}$$

The transformation (4.20c) depends on the parameter x_c. It is chosen as $x_c = f(-d)$. With this choice $f(z) \leq p/4 = 0.25\mu m < f_{\max} \approx 0.387\mu m$ in the domain $-d \leq z \leq 0$ and the transformation is invertible (equation (4.28)). Furthermore, the choice $x_c = f(-d)$ ensures continuity at the interface $z_{\min} = -d$ to free space in the sense of equation (4.21) because then $f(-d) = x_c \overset{(4.26)}{\Rightarrow} a_3(-d) = 0 \overset{(4.24)}{\Rightarrow} a_1(-d) = 1 \overset{(4.23)}{\Rightarrow} t(x,-d) = x$. To accomplish continuity at the other boundary, it is necessary to extend the transformation beyond the original grating boundary, $0 < z_{\max}$, and transfer $t(x,z)$ to the identity at $z = z_{\max}$. The choice $z_{\max} = d$ and the use of $f(z) = f(|z|)$ extend the transformation symmetrically beyond $z = 0$, such that $f(d) = x_c \Rightarrow t(x,d) = x$. The components of the permittivity and permeability tensors calculated with the equations (4.30)-(4.35) are depicted in the figures 4.5 and 4.6.

Since the transformation leaves the regions $z < z_{\min}$, $z_{\max} < z$ unchanged and is continuous everywhere else, the transmitted light in the region $z_{\max} < z$ and the reflected light in the region $z < z_{\min}$ should be identical for both gratings if they are irradiated by the same light. To check this, I solve Maxwell's equations numerically for both gratings as a one-dimensional grating problem (section 3.1), with outgoing wave boundary condition (section

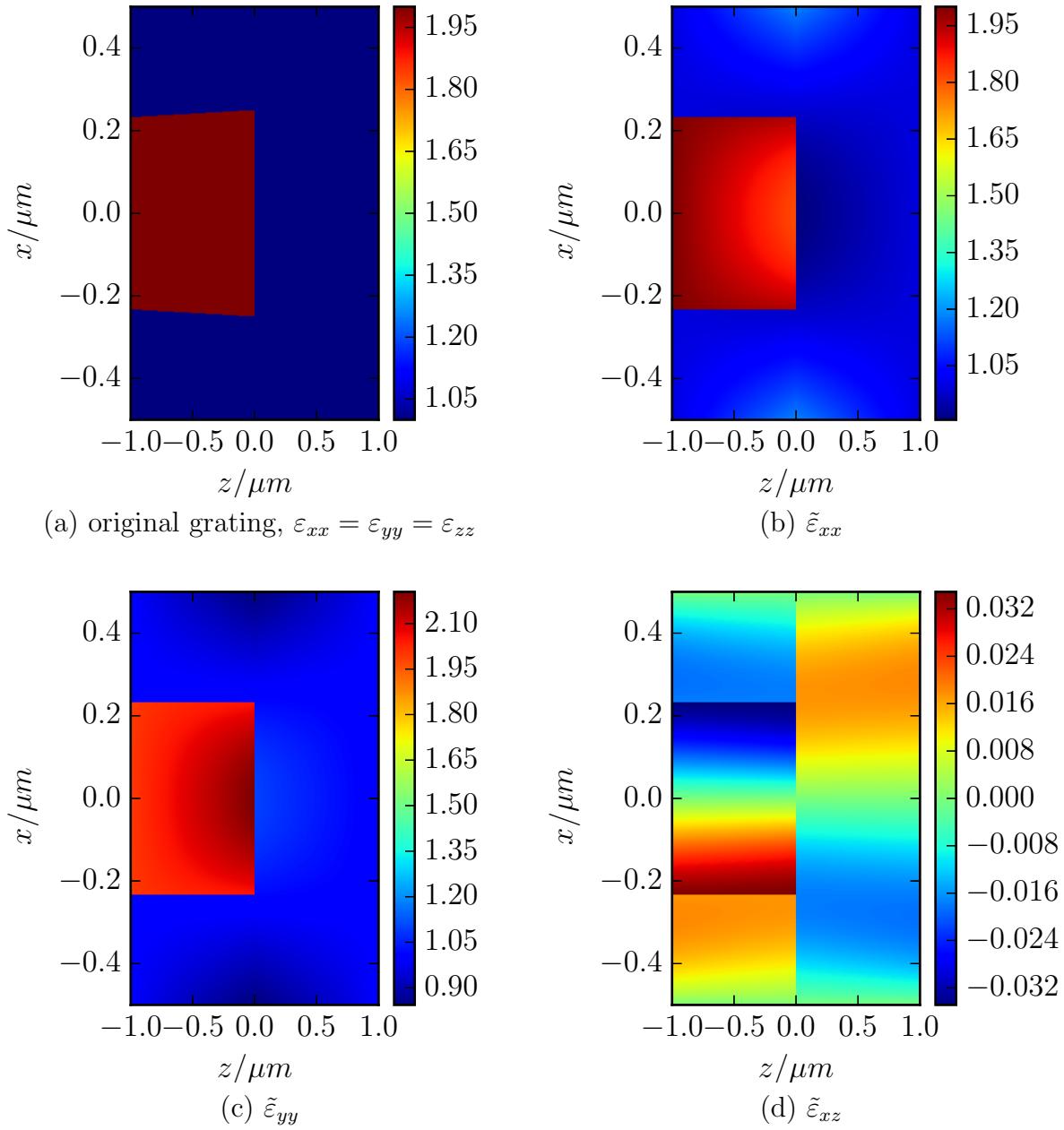

(a) original grating, $\varepsilon_{xx} = \varepsilon_{yy} = \varepsilon_{zz}$ (b) $\tilde{\varepsilon}_{xx}$

(c) $\tilde{\varepsilon}_{yy}$ (d) $\tilde{\varepsilon}_{xz}$

Figure 4.5: Scalar permittivity of the original grating with linear contour $f(z) = p/4 - \tan(1°)\,|z|$ and the components of the permittivity tensors of the transformed grating, $\tilde{\varepsilon}$. Note that $z_{\min} = -d$ and $z_{\max} = d$, where $d = 1\mu m$.

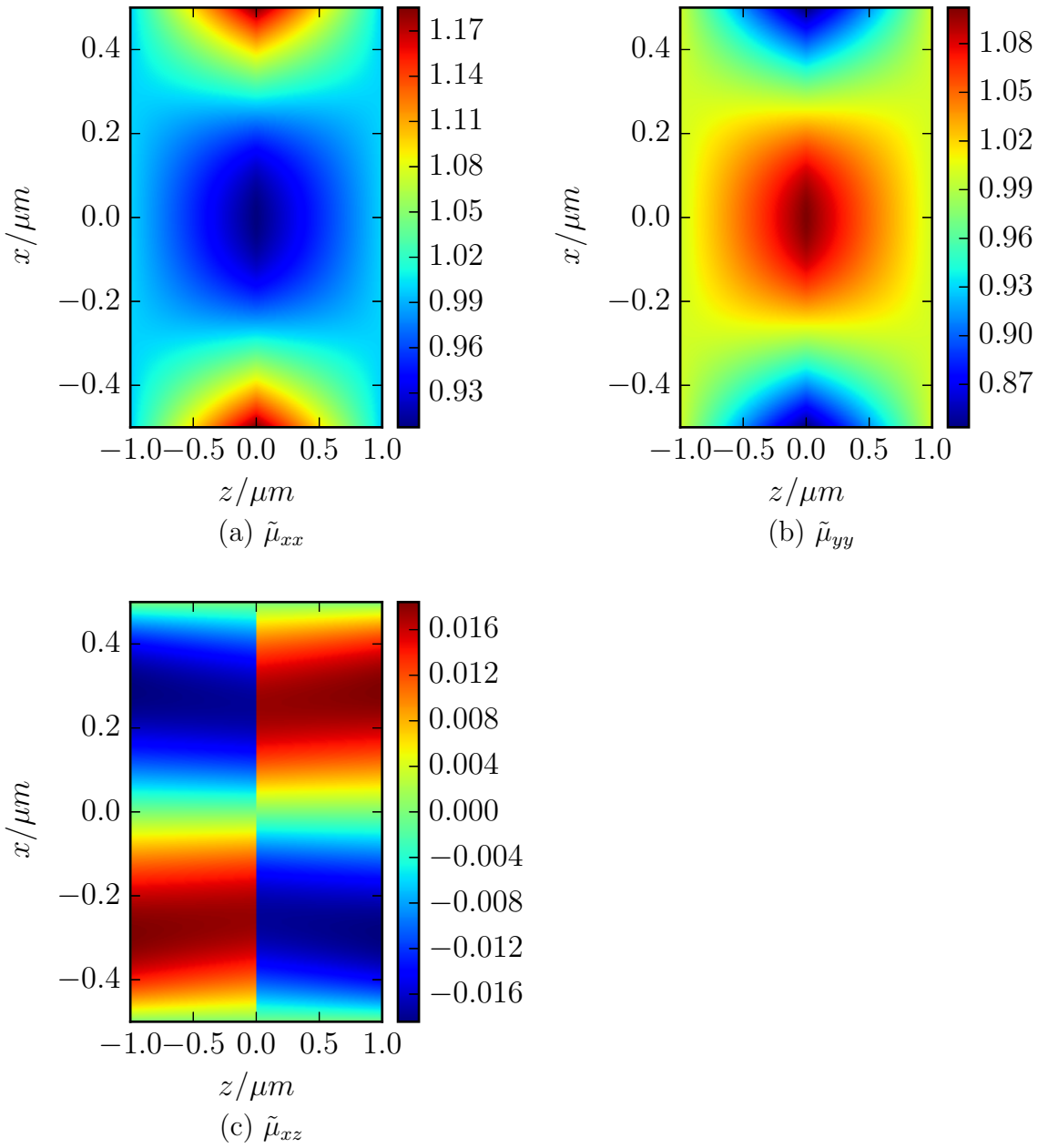

Figure 4.6: The components of the relative permeability tensors of the transformed grating, $\tilde{\mu}$, with the original grating as shown in figure 4.5(a).

3.3) by means of the differential method (section 3.2) in combination with the S-matrix propagation algorithm explained in section 3.4.3. This implies assuming periodicity in the x-direction.

On the left boundary, a perpendicularly incident plane wave with wavelength $\lambda = 0.633\mu m$, amplitude $1V/m$ and linearly polarised in the y-direction is chosen as boundary condition:

$$R(d) = 0, \tag{4.37}$$

$$T_{xm}(-d) = 0, \quad \forall\, m \in \{-N, \ldots, N\} \tag{4.38}$$

$$T_{ym}(-d) = \begin{cases} 1, & \text{if } m = 0 \\ 0, & \text{else,} \end{cases} \tag{4.39}$$

and $k_{x,0} = 0$.

For the differential method, I calculate the matrix M of the differential equation (3.5) in the way described by Watanabe, Petit and Nevière in 2002 [30, equation 65] with the same modifications as in section 4.1. But this time the Fourier coefficients of the material functions are calculated differently. The material functions of the original grating are constant or rectangular functions whose Fourier coefficients are analytically known, hence I use them. Since, I do not know the analytical coefficients for the transformed grating, I resort to numerical coefficients.

To solve the boundary value problem I use the S-matrix propagation algorithm (3.39) (3.43) with 256 subdomains. On inhomogeneous subdomains the transfer matrices are calculated with the basis mapping technique (3.20) explained at the end of section 3.4.2. I numerically integrate the basis (3.21) over these subdomains with the Runge-Kutta-Prince-Dormand(8,9) method plus adaptive stepsize control using routines from the GNU scientific library (GSL) [66, chapter 25, "ordinary differential equations"; in the more current version 2.4 of this manual it is chapter 27]. Adaptive stepsize control estimates the error done in every integration step and adapts the stepsize according to a desired error threshold [54, section 81] [39, section 17.2]. I set desired error threshold with the "gsl_odeiv2_control_standard_new" routine [66] using the absolute error $\epsilon_{\text{rel}} = 10^{-6}$, the relative error $\epsilon_{\text{abs}} = 10^{-6}$ and the scaling factors $a_y = 1 = a_{\text{dydt}}$. Additionally, I use the discrete Fourier transformations routines of the GSL and its interface to the BLAS for several linear algebra operations and the routines "zgetrf", "zgetri" of LAPACK [67] for matrix inversions. The $2N + 1$ numerical coefficients for the material functions are calculated by evaluating them on a equidistant grid of 16384 points over one period. The subsequent DFT yields vectors of size 16384 that are truncated to the size $2N + 1$.

With the solutions for both perpendicularly irradiated gratings, I calculate the diffraction efficiencies with [37, equation 25] [34, equation 1.50]

$$\mathrm{DE}(T_m) = T_m T_m^* \, \frac{\cos\theta_n}{\cos\theta_0} \overset{\theta_0=0}{\underset{\text{here}}{=}} T_m T_m^* \, \mathrm{Re}\left(k_{z,m}/k_0\right), \tag{4.40}$$

for modes T_k transmitted with an angle θ_n into the vacuum region $d = z_{\max} \leq z$. These efficiencies correspond to the power fluxes of the diffraction orders [34, section 1.2.3]. The zeroth and the first diffraction order are the only propagative modes. The others are evanescent and carry no energy in the z-direction [68, section 3.10.2].

The diffraction efficiencies for the original grating and the transformed grating are shown in figure 4.7 for increasing truncation level N. For a quite low truncation level of $N = 10$ the diffraction efficiencies converge to almost the same values. A more sensitive measure for the difference between the solutions in the isotropic zones is

$$\Delta S := \left\| S(z_{\min}) - \tilde{S}(z_{\min}) \right\|_1 + \left\| S(z_{\max}) - \tilde{S}(z_{\max}) \right\|_1, \tag{4.41}$$

with $S = \begin{pmatrix} T \\ R \end{pmatrix}$. This measure takes into account phase factors and evanescent modes, in contrast to the diffraction efficiencies (4.40). The black diamonds in the plot 4.8 show this measure ΔS with increasing truncation level N. The other curves show the same measure for other simulations. These simulations differ from the previous ones only in the number of sampling points used to numerically calculate the Fourier coefficients of the material functions. Several observations can be made with these results. One is that the agreement of the theory with the numerical results is not as good as in section 4.1 where a very similar measure of difference is used and values around 10^{-11} are achieved (4.16). This is magnitudes lower than the lowest values of ΔS achieved here. The method used here has more numerical error sources but a limited of "adjusting screws" that control its accuracy. The truncation level N is not too low. This can be seen in figure 4.8 from the plateau behaviour ΔS. Increasing the truncation level on the plateau does not give a better agreement between the original and the transformed diffraction grating. The other observation is that the height and the beginning of the ΔS-plateau depend on the number of sampling points.

Using numerical Fourier coefficients is not exact. To estimate the error due to the use of numerical coefficients, I determine ΔS between two solutions of the original grating. One of the solutions is calculated with analytical coefficients. The other solution is calculated with numerical coefficients obtained from 8192 sampling points. Then, with a truncation level of $N = 66$,

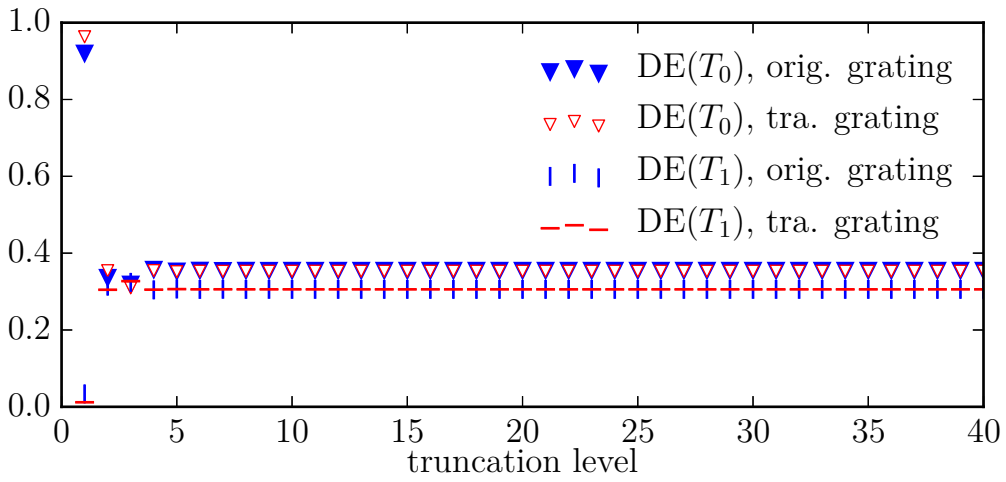

Figure 4.7: Transmitted diffraction efficiencies of the original grating with linear contour $f(z) = p/4 - \tan(1°)\,|z|$ and the diffraction efficiencies of the transformed grating with respect to the truncation level N.

the measure of difference is $\Delta S \approx 9.4\ 10^{-6} \approx 10^{-5}$. This is still lower than the lowest value for $\Delta S \approx 10^{-4}$ in figure 4.8.

There are other error sources. The Newton method used in the inverse transformation is one of them. This method is an iteration that stops when the residual $t(x) - x' < \mathrm{TOL} =: 10^{-15}$. With such a low TOLerance the contribution of the numerical inversion to the overall error should be negligible. The 256 subdomains used in the S-matrix algorithm should be more than enough to avoid ill-conditioned matrix inversions due to the stiffness of the ODE. The transfer matrices of the subdomains are calculated by means of a numerical integration. The error in this numerical integration should be bounded by the use of the adaptive stepsize routine. But what it really controls is only an estimate of the error in each step using a predefined error threshold. And the error threshold in each step is determined by the parameters I feed the routine with. These parameters, the number of sampling points for the Fourier coefficients, the number of subdomains used in the S-matrix algorithm and the tolerance of the Newton method are the "adjusting screws" that influence the accuracy of the numerical method used. Adjusting these one could further improve the agreement of the diffraction efficiencies (4.40) or lower the measure ΔS (4.41).

But changing the physical properties of the problem is more interesting. The original grating is isotropic and binary in the sense of equation (4.19) in contrast to the transformed grating which is anisotropic and not binary. But the permittivity and permeability distributions of the transformed grating do

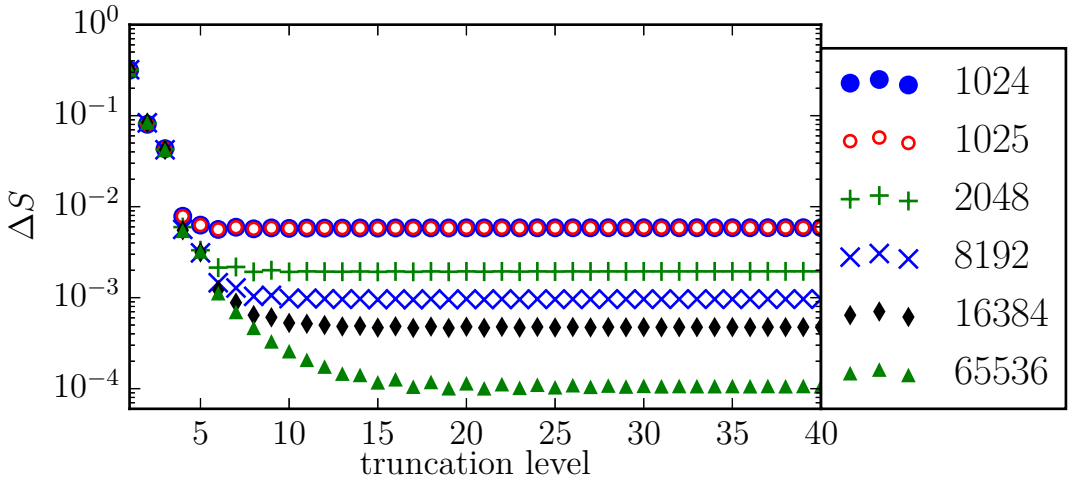

Figure 4.8: The measure $\Delta S/(V/m)$ (4.41) with respect to the truncation level and for different number of sampling points in the numerical calculation of Fourier coefficients of the material functions.

not deviate that much from those of the original grating as can be seen in the figures 4.5, 4.6. The reason is that the transformation distorts the grating domain only slightly. This is due to the low variations of the contour $f(z)$ and the choice $x_c = f(-d)$. The practically equivalent diffraction behaviour between both gratings would be more meaningful if the transform distorted the grating domain more extremely. Such more distorting transformations are studied in the next two sections. In both of them, this is accomplished with contours $f(z)$ that are highly varying as compared to (4.42). Apart from that, these following sections are conceptually and methodologically similar to this section.

4.2.2 Straightening of a linear contour of higher variation

Let the contour function $f(z)$ be defined as

$$f(z) = p/4 - \tan(10°)\ |z|, \tag{4.42}$$

and the transformation that straightens this contour is determined by the choices $x_c = f(-d)$, $z_{\min} = -d$ and $z_{\max} = d$. These choices ensure continuity of the transformation (4.23) at the boundaries $z_{\min}$, $z_{\max}$. An explanation is given in section 4.2.1. The period $p = 1\mu m$ and the thickness $d = 1\mu m$. With these choices, $f(z) \leq p/4 = 0.25\mu m < f_{\max} \approx 0.26\mu m$ in the domain

$z_{\min} \leq z \leq z_{\min}$ and hence the transformation (4.23) is invertible (equation (4.28)). The components of the permittivity and permeability tensors calculated with the equations (4.30)-(4.35) are depicted in the figures 4.9 and 4.10.

This time, the transformed grating barely resembles the original grating. In particular, the component $\tilde{\varepsilon}_{yy}$ shown in 4.9(c) features a very high peak in the center rendering the original contour almost invisible with the linear scale used. One can still recognise the contour in the other plots 4.9(b), 4.9(d), though.

In order to check whether both gratings diffract light equivalently, I apply the same procedure as used in section 4.2.1: Maxwell's equations are solved with the same boundary conditions 4.37 by means of the differential method in combination with the S-matrix algorithm.

Some computational details are different, though. These details are given in this paragraph. For the transformed grating, the number of sampling points used to numerically calculate the Fourier coefficients of the material functions is 8192. The number of subdomains in the S-matrix algorithm is 512 and the transfer matrices of these subdomains are calculated in exactly the same way as done in section 4.2.1. What follows concerns the original grating. For the original grating, the staircase approximation [69] is used. This means that the grating is treated as a stack of homogeneous layers. I use 512 of these layers as the subdomains in the S-matrix algorithm. And in each subdomain $[z_k, z_{k+1}]$ I calculate the transfer matrix in one step by means of the diagonalisation technique [40, section 1.3]:

$$\check{T}_k = Q^{-1} V_k^{-1} \exp(i D_k (z_k - z_{k+1})) V_k Q, \tag{4.43}$$

where Q is the conversion matrix (A.21). The diagonal matrix D_k consists of the eigenvalues of $M_k := M\left((z_k + z_{k+1})/2\right)$, where $M(z)$ is the matrix of the ODE (3.5). And the matrix V contains the eigenvectors of M such that $M_k = V_k^{-1} D_k V_k$. I use the LAPACK routine "zgeev" [67] for the diagonalisations. This approximation and the fact that no adaptive stepsize control is used here make this technique error-prone. But not with so many layers. The advantage is the predictable execution time.

With the solutions for both perpendicularly irradiated gratings, I calculate the diffraction efficiencies with equation (4.40) and the measure ΔS with equation (4.41). The diffraction efficiencies for the original grating and the transformed grating are shown in figure 4.11 while the measure ΔS is depicted in figure 4.12. In contrast to the simulations in the previous section 4.2.1, a truncation level of $N = 10$ is not enough to achieve a reasonable convergence of the diffraction efficiencies. But they do converge to almost

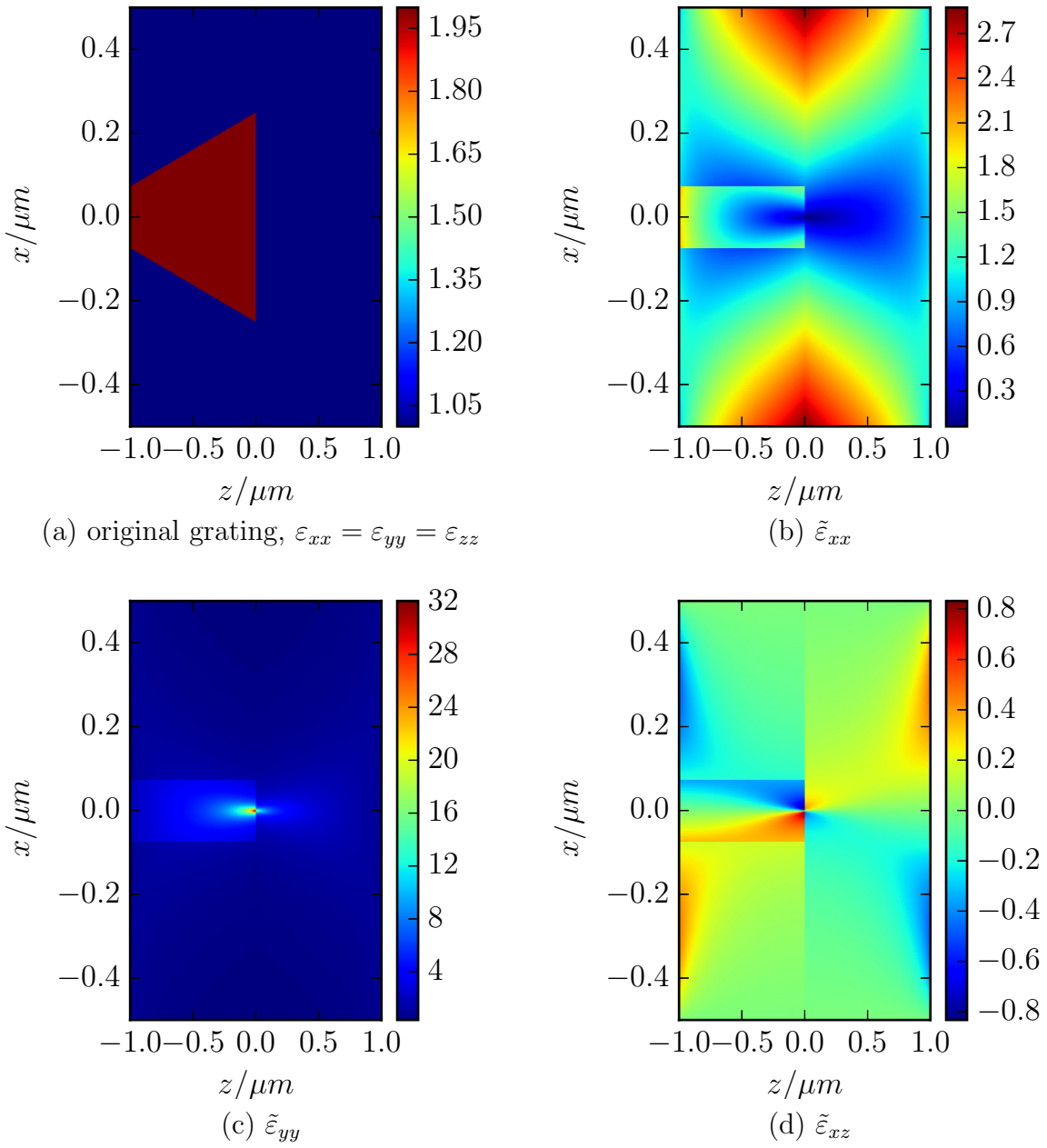

(a) original grating, $\varepsilon_{xx} = \varepsilon_{yy} = \varepsilon_{zz}$ (b) $\tilde{\varepsilon}_{xx}$

(c) $\tilde{\varepsilon}_{yy}$ (d) $\tilde{\varepsilon}_{xz}$

Figure 4.9: Scalar permittivity of the original grating with linear contour $f(z) = p/4 - \tan(10°)\ |z|$ and the components of the permittivity tensors of the transformed grating, $\tilde{\varepsilon}$. Note that $z_{\min} = -d$ and $z_{\max} = d$, where $d = 1\mu m$.

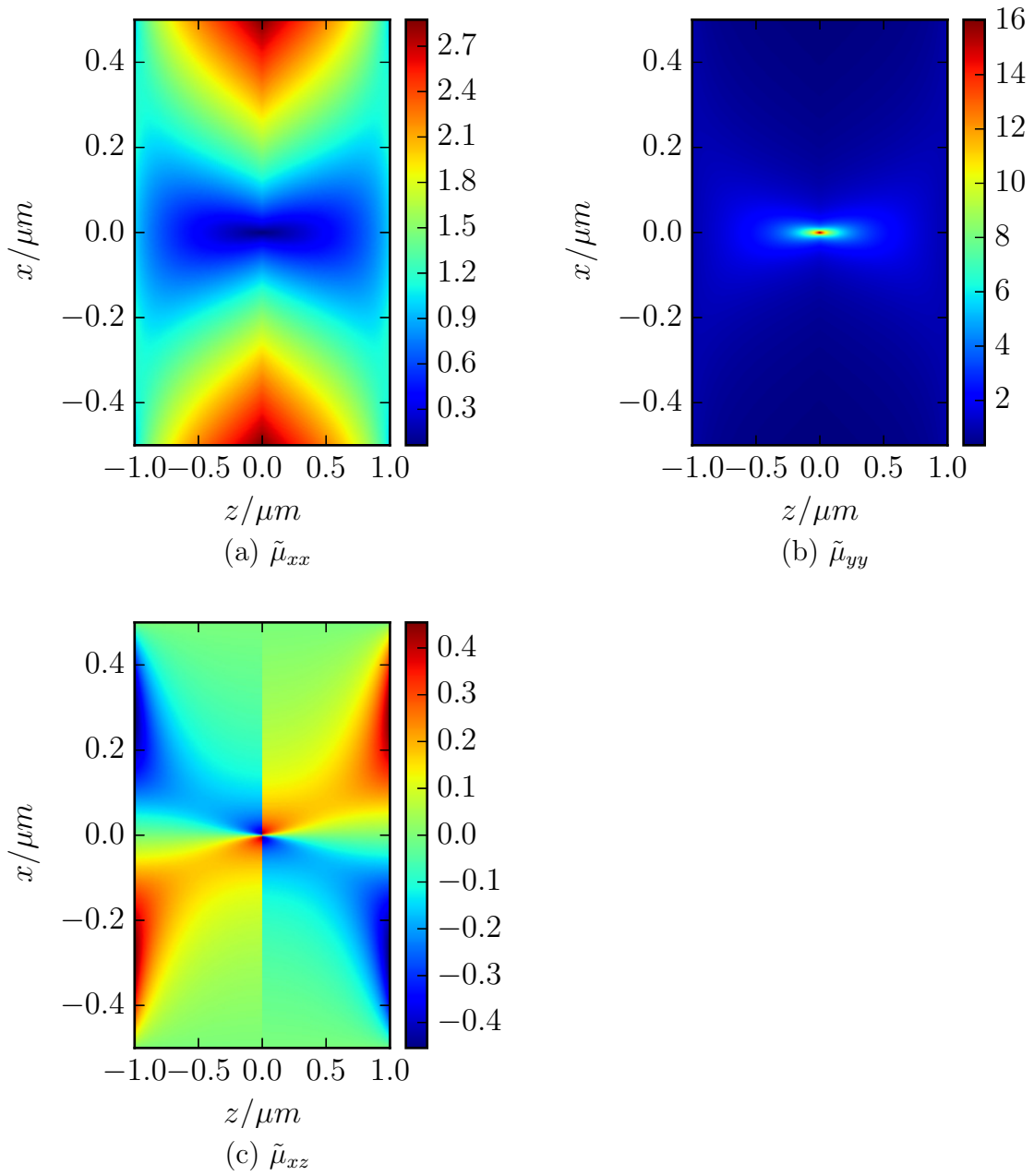

(a) $\tilde{\mu}_{xx}$ (b) $\tilde{\mu}_{yy}$

(c) $\tilde{\mu}_{xz}$

Figure 4.10: The components of the relative permeability tensors of the transformed grating, $\tilde{\mu}$, with the original grating as shown in figure 4.9(a).

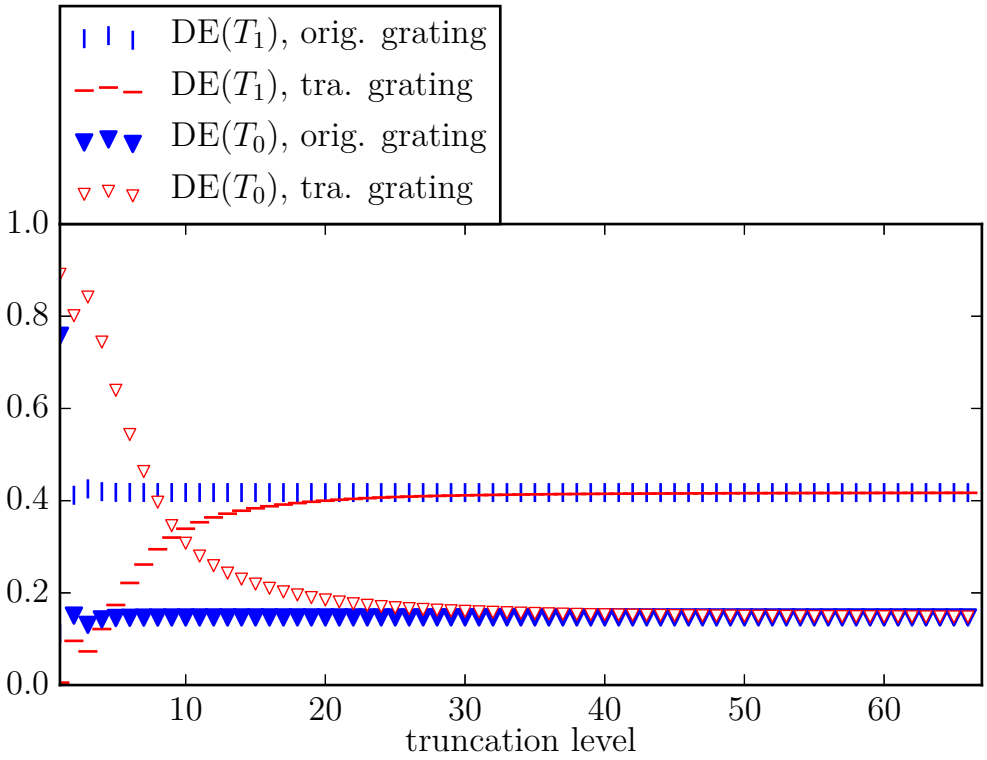

Figure 4.11: Transmitted diffraction efficiencies of the original grating with linear contour $f(z) = p/4 - \tan(10°)\,|z|$ and the diffraction efficiencies of the transformed grating with respect to the truncation level N.

the same values at $N = 60$. The more sensitive measure difference ΔS (figure 4.12) reveals that a truncation level of around 200 is necessary to reach the plateau. The height of this plateau is around 10^{-4} which is comparable to those obtained in the previous section 4.2.1.

4.2.3 Straightening of a sine contour

The concept evolved in section 4.2 is not restricted to linear contour functions. It is restricted to continuous contours that obey equation (4.28). Let the contour function $f(z)$ be defined as

$$f(z) = p/4 + A\sin(k_f z), \tag{4.44}$$

where $A = 0.5\mu m$ and $k_f = 2\pi/\mu m$, the period $p = 10\mu m$ and the thickness $d = 1\mu m$. The transformation that straightens this contour is determined by the choices $x_c = f(-d)$, $z_{\min} = -d$ and $z_{\max} = 0$. Since

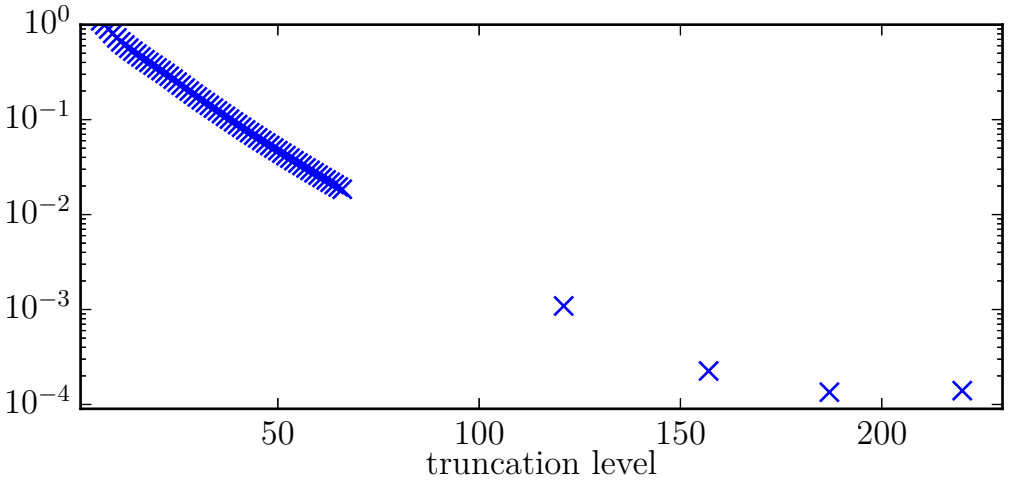

Figure 4.12: The measure $\Delta S/(V/m)$ (4.41) with respect to the truncation level for the highly varying linear contour as original grating.

$f(-d) = f(0)$, it is not necessary to extend the transformation beyond the original grating domain to render it continuous. Furthermore, the transformation (4.23) that straightens this contour is invertible (equation (4.28)) because $f(z) \leq p/4 + A = 3\mu m < f_{\max} \approx 3.97\mu m$.

The components of the permittivity and permeability tensors calculated with the equations (4.30)-(4.35) are depicted in the figures 4.13, 4.14. Like the contour of the previous section (4.42) this sine contour (4.44) varies much. The component $\tilde{\mu}_{xx}$ and the off-diagonal components $\tilde{\mu}_{xz}$ of the transformed permeability tensor feature high peaks at the turning points of the contour function $f(z)$. These peaks are by no means as sharp as the peaks in figure 4.10(b) caused by the highly varying linear contour. But for increasing amplitude A these peaks become higher and higher.

Since the period is ten times bigger than in the previous sections 4.2.1, 4.2.2, there are more propagative modes in the isotropic homogeneous zones and hence more diffraction efficiencies available to compare. Several diffraction efficiencies of transmitted modes in $0 \leq z$ as well as the efficiencies of reflected modes in $z \leq 0$ are plotted in figure 4.15, with respect to the truncation level. All of them converge to almost the same values at a truncation level $N = 50$. These results confirm the claim in the beginning of this section: The concept is not restricted to linear contours. Apart from that, I gained no additional insight here.

To obtain these results I apply the same procedure in section 4.2.1: Maxwell's equations are solved with the same boundary conditions 4.37 by means of the differential method in combination with the S-matrix algo-

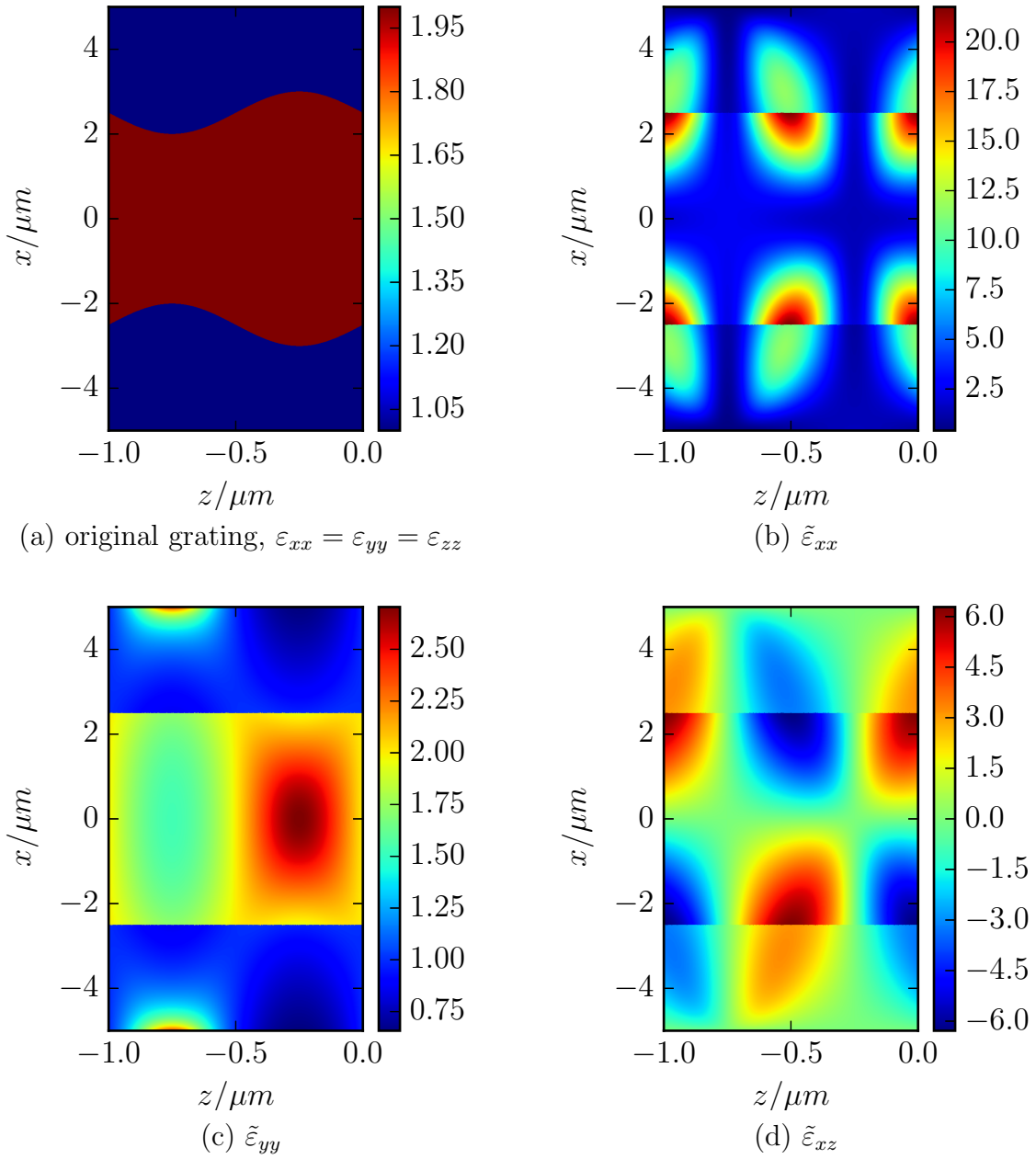

(a) original grating, $\varepsilon_{xx} = \varepsilon_{yy} = \varepsilon_{zz}$

(b) $\tilde{\varepsilon}_{xx}$

(c) $\tilde{\varepsilon}_{yy}$

(d) $\tilde{\varepsilon}_{xz}$

Figure 4.13: Scalar permittivity of the original grating with sine contour $f(z) = p/4 + A\sin(k_f z)$ and the components of the permittivity tensor of the transformed grating, $\tilde{\varepsilon}$.

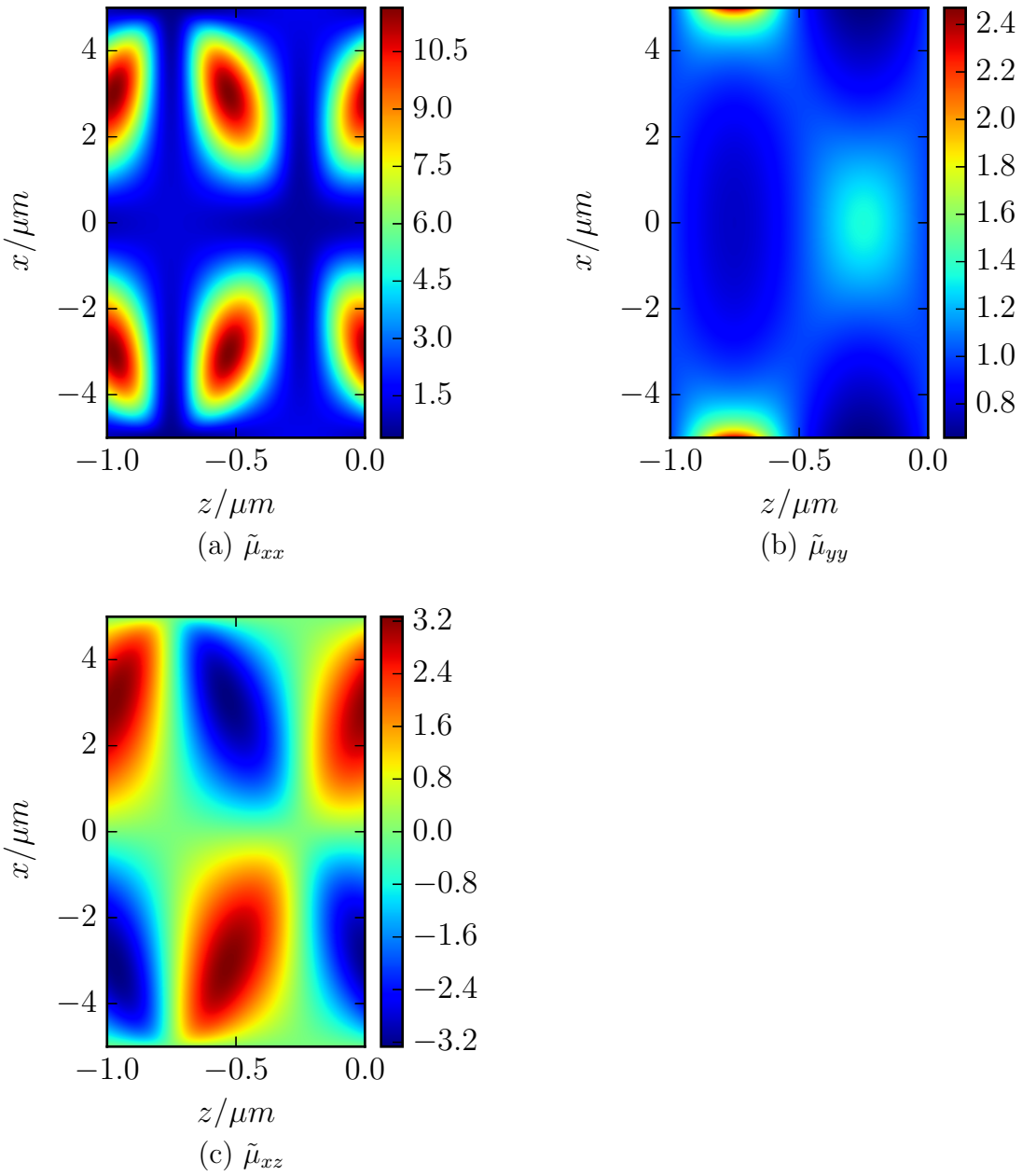

(a) $\tilde{\mu}_{xx}$ (b) $\tilde{\mu}_{yy}$

(c) $\tilde{\mu}_{xz}$

Figure 4.14: The components of the relative permeability tensors of the transformed grating, $\tilde{\mu}$, with the original grating as shown in figure 4.13(a).

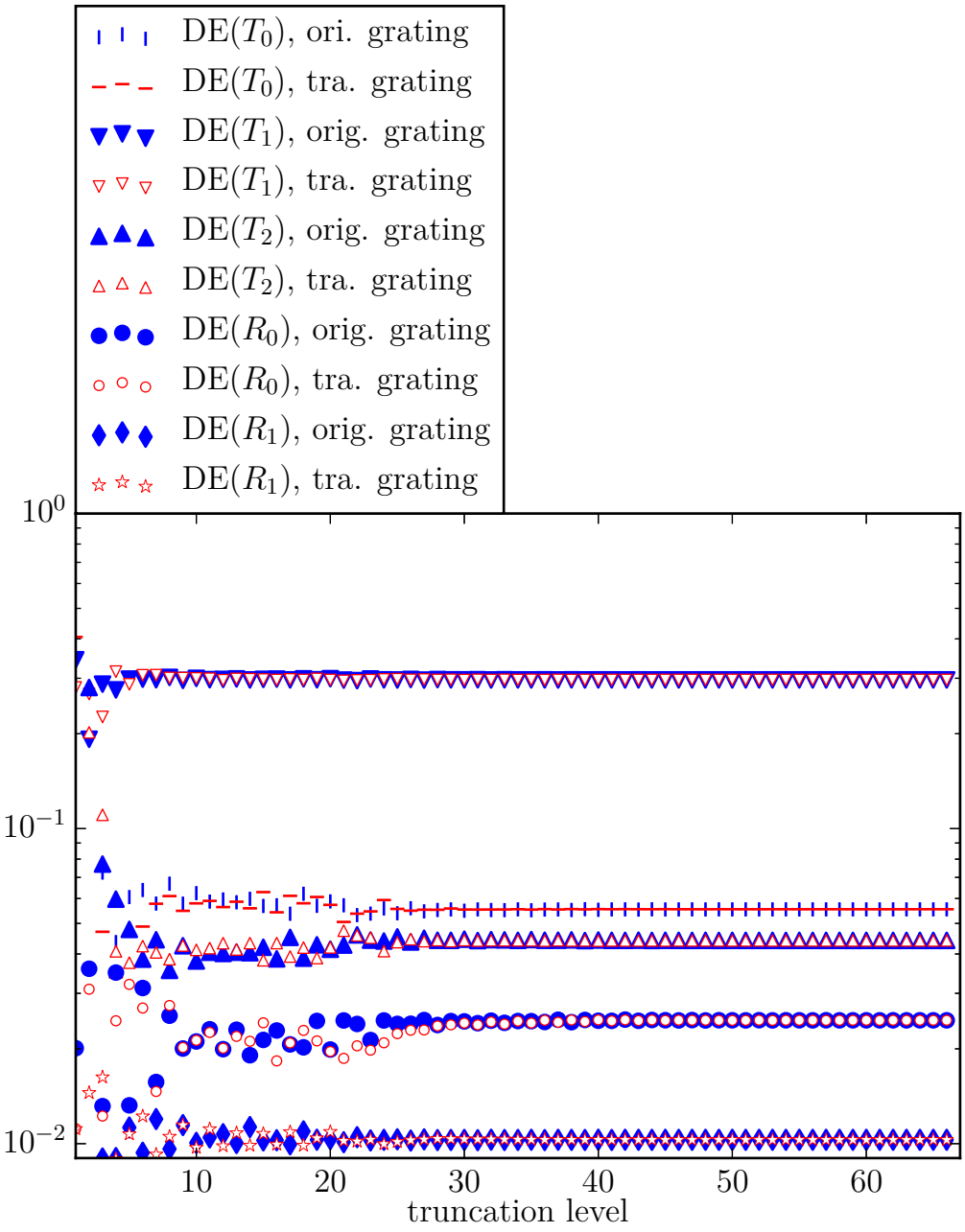

Figure 4.15: Several diffraction efficiencies of the original grating with contour $f(z) = p/4 + A\sin(k_f z)$ and diffraction efficiencies of the transformed grating with respect to the truncation level N.

rithm. The computational details that deviate from the previous section are the following. For the original grating, the number of subdomains in the S-matrix algorithm is 512 and the transfer matrices are obtained by numerical integration, in the same way as in section 4.2.1. The transformed grating is approximated with 1024 homogeneous layers and the transfer matrix for each layer is calculated with the diagonalisation technique explained in section 4.2.2.

Chapter 5

Summary

This work gives an introduction to the field of transformation optics in the section "transformation optics" and a derivation of the transformation rules. These transformation rules are used to obtain the permittivity and permeability tensors of transformed gratings in the section "transformed gratings".

The study of these transformed gratings makes use of the methods in the section "methods for the grating problem". There, I try to shed light on two fundamental issues of the differential method and related methods: memory and stiffness. I further provide explanations how and why the two algorithms presented in this section solve the stiffness problem. The multiple shooting method has parallelisation potential and there are numerous ways to solve the root finding problem arising in the multiple shooting method. I suppose that this freedom could be used to alleviate the memory problem. The S-matrix algorithm is recursive and recursions cannot be parallelised.

The results of the "transformed gratings" section allow for the following conclusion: Given any grating, there is an infinite number of other gratings that exhibit the very same diffraction behaviour. The design of such equivalent gratings mainly consists of finding continuous invertible transformations, of which there are infinitely many.

A transformation of the axial direction is the simplest way to accomplish this. The axial linear transformation applied to a diffractive optical element in section 4.1 is just one of them. If the lateral direction shall be transformed, some difficulties arise. These difficulties and how to counter them are treated in section 4.1. There, gratings defined by a contour are transformed in a way that maps the contour to a constant. The equivalence of the transformed gratings with the original one is studied with the numerical solution of Maxwell's equations. If numerical errors are ignored, the numerical results confirm equivalent diffraction behaviour in all the cases studied.

Appendix A

The conversion matrix

In this section, the matrix Q that converts between the field vector F and the propagation vector $S = \begin{pmatrix} T \\ R \end{pmatrix}$ is derived for homogeneous isotropic material:

$$F := \begin{pmatrix} [E_x] \\ [E_y] \\ [H_x] \\ [H_y] \end{pmatrix} = \begin{pmatrix} 1 & 1 \\ Q_{21} & Q_{22} \end{pmatrix} S := Q \begin{pmatrix} T \\ R \end{pmatrix} := Q \begin{pmatrix} [T_x] \\ [T_y] \\ [R_x] \\ [R_y] \end{pmatrix}. \tag{A.1}$$

The propagation vector consists of the amplitudes of plane waves in the Rayleigh expansion of the electrical field. The first row of Q consists of unit matrices by definition. What remains is a conversion matrix C that converts S to the Fourier modes of $[H_x]$ and $[H_y]$. This conversion can also be found elsewhere [51] [32, section 7.3] [23, section 3.3.2.5]. In the truncated Fourier expansion with respect to x of the electrical field (3.2)

$$\begin{pmatrix} E_x(x,z) \\ E_y(x,z) \end{pmatrix} = \sum_{m=-N}^{N} \begin{pmatrix} E_{xm}(z) \\ E_{xm}(z) \end{pmatrix} e^{ik_{x,m}x}, \quad k_{x,m} = k_{x,0} + m\frac{2\pi}{d}, \tag{A.2}$$

the information about the propagation in the z-direction is in the $\begin{pmatrix} E_{xm}(z) \\ E_{xm}(z) \end{pmatrix}$ part. And in a homogeneous isotropic region, this part can be expanded as well [34, section 1.2.3]

$$\begin{pmatrix} E_x(x,z) \\ E_y(x,z) \end{pmatrix} = \sum_{m=-N}^{N} \left(\begin{pmatrix} T_{xm}(z_0) \\ T_{ym}(z_0) \end{pmatrix} e^{ik_{z,m}(z-z_0)} + \begin{pmatrix} R_{xm}(z_0) \\ R_{ym}(z_0) \end{pmatrix} e^{-ik_{z,m}(z-z_0)} \right) e^{ik_{x,m}x}, \tag{A.3}$$

$$k_{x,m} = k_{x,0} + m\frac{2\pi}{d}, \quad k_{z,m} = \sqrt{\omega^2\varepsilon\mu - k_{x,m}^2}, \tag{A.4}$$

with the permittivity ε and the permeability μ in this region and the wave number $k_{z,m}$ that follows from

$$k_x^2 + k_z^2 = k^2 = \left(\frac{2\pi}{\lambda}\right)^2 n = \omega^2 \varepsilon \mu, \tag{A.5}$$

where k_x is the x-component of the wave vector k and k_z is its z-component. The y-component of the wave vector is zero because the waves travel in a direction perpendicular to the y-axis by definition. The number n is the refractive index of the material in the homogeneous region. In the plane-wave expansion (3.3), sometimes called Rayleigh expansion, the waves are split into R (reflection) and T (transmission) according to their direction of propagation.

So, comparing the two equations (A.2) and (3.3) gives

$$\begin{pmatrix} E_{xm}(z) \\ E_{ym}(z) \end{pmatrix} = \left(\begin{pmatrix} T_{xm}(z_0) \\ T_{ym}(z_0) \end{pmatrix} e^{ik_{z,m}(z-z_0)} + \begin{pmatrix} R_{xm}(z_0) \\ R_{ym}(z_0) \end{pmatrix} e^{-ik_{z,m}(z-z_0)} \right), \tag{A.6}$$

and the choice $z_0 = z$ yields

$$\begin{pmatrix} E_{xm}(z) \\ E_{ym}(z) \end{pmatrix} = \left(\begin{pmatrix} T_{xm}(z) \\ T_{ym}(z) \end{pmatrix} + \begin{pmatrix} R_{xm}(z) \\ R_{ym}(z) \end{pmatrix} \right), \tag{A.7}$$

that is, the trivial conversion between the components of the propagation vector S and the modes of the electrical field $[E_x], [E_y]$. What remains is to get a similar expression for the modes of the magnetic field. The rotational Maxwell equations in Cartesian coordinates read

$$\mathrm{rot} E = i\omega\mu H, \quad \mathrm{rot} H = -i\omega\varepsilon E. \tag{A.8}$$

The considered problem is invariant in the y-direction, hence $\partial_y E = 0 = \partial_y H$ and some entries in the equations (A.8) are zero

$$i\omega\mu H = \begin{pmatrix} -\partial_z E_y \\ \partial_z E_x - \partial_x E_z \\ \partial_x E_y \end{pmatrix}, \tag{A.9}$$

$$-i\omega\varepsilon E = \begin{pmatrix} -\partial_z H_y \\ \partial_z H_x - \partial_x H_z \\ \partial_x H_y \end{pmatrix}. \tag{A.10}$$

Let us consider the first component of equation (A.9). Here, we can expand the fields on both sides of the equation as in (A.2) which gives

$$i\omega\mu H_{xm} = -\partial_z E_{ym}. \tag{A.11}$$

On the right side of this equation we can insert (A.6) and apply the derivative

$$i\omega\mu H_{xm}(z) = -\partial_z \left(T_{ym}(z_0) e^{ik_{z,m}(z-z_0)} + R_{ym} e^{-ik_{z,m}(z-z_0)} \right), \tag{A.12}$$

$$= \left(-ik_{z,m} T_{ym} e^{ik_{z,m}(z-z_0)} + ik_{z,m} R_{ym} e^{-ik_{z,m}(z-z_0)} \right), \tag{A.13}$$

and rearrange them slightly

$$H_{xm}(z) = \frac{k_{z,m}}{\omega\mu} \left(-T_{ym} e^{ik_{z,m}(z-z_0)} + R_{ym} e^{-ik_{z,m}(z-z_0)} \right), \tag{A.14}$$

and choose $z = z_0$

$$H_{xm}(z) = \frac{k_{z,m}}{\omega\mu} \left(-T_{ym}(z) + R_{ym}(z) \right). \tag{A.15}$$

So, the conversion for one magnetic field component is done. The second follows at once. Let us have a look at the second component of equation (A.9)

$$i\omega\mu H_y = \partial_z E_x - \partial_x E_z, \tag{A.16}$$

and eliminate E_z using the third component of equation (A.10)

$$i\omega\mu H_y = \partial_z E_x - \partial_x E_z = \partial_z E_x + \frac{1}{i\omega\varepsilon} \partial_x^2 H_y, \tag{A.17}$$

and insert the truncated Fourier expansions and apply the derivatives

$$\begin{aligned}
i\omega\mu \sum_{m=-N}^{N} H_{ym}(z) e^{ik_{x,m}x} &= \sum_{m=-N}^{N} \left(\partial_z E_{xm}(z) + \frac{1}{i\omega\varepsilon} \partial_x^2 H_{ym}(z) \right) e^{ik_{x,m}x} \\
&= \sum_{m=-N}^{N} \left(\partial_z E_{xm}(z) + \frac{ik_{x,m}^2}{\omega\varepsilon} H_{ym}(z) \right) e^{ik_{x,m}x} \\
&= \sum_{m=-N}^{N} \left(\partial_z \left(T_{xm}(z) e^{ik_{z,m}(z-z_0)} - R_{xm}(z) e^{-ik_{z,m}(z-z_0)} \right) + \frac{ik_{x,m}^2}{\omega\varepsilon} H_{ym}(z) \right) e^{ik_{x,m}x} \\
&= \sum_{m=-N}^{N} \left(ik_{z,m} T_{xm}(z) e^{ik_{z,m}(z-z_0)} - ik_{z,m} R_{xm}(z) e^{-ik_{z,m}(z-z_0)} + \frac{ik_{x,m}^2}{\omega\varepsilon} H_{ym}(z) \right) e^{ik_{x,m}x},
\end{aligned} \tag{A.18}$$

hence

$$\left(i\omega\mu - \frac{ik_{x,m}^2}{\omega\varepsilon} \right) H_{ym}(z) = ik_{z,m} \left(T_{xm}(z) e^{ik_{z,m}(z-z_0)} - R_{xm}(z) e^{-ik_{z,m}(z-z_0)} \right), \tag{A.19}$$

and with the choice $z = z_0$

$$H_{ym}(z) = \frac{k_{z,m}}{\omega\mu - \frac{k_{x,m}^2}{\omega\varepsilon}} \left(T_{xm}(z) - R_{xm}(z)\right) = \frac{\omega\varepsilon}{k_{z,m}} \left(T_{xm}(z) - R_{xm}(z)\right). \quad \text{(A.20)}$$

This equation, put together with (A.15) and (A.7) is the complete conversion and reads

$$\begin{pmatrix} E_{xm} \\ E_{ym} \\ H_{xm} \\ H_{ym} \end{pmatrix} = \begin{pmatrix} T_{xm} \\ T_{ym} \\ -\frac{k_{z,m}}{\omega\mu} T_{xm} \\ \frac{k_{z,m}}{\omega\mu} T_{ym} \end{pmatrix} + \begin{pmatrix} R_{xm} \\ R_{ym} \\ \frac{\omega\varepsilon}{k_{z,m}} R_{xm} \\ -\frac{\omega\varepsilon}{k_{z,m}} R_{ym} \end{pmatrix} = \begin{pmatrix} 1 & 0 & 1 & 0 \\ 0 & 1 & 0 & 1 \\ 0 & -\frac{k_{z,m}}{\omega\mu} & 0 & \frac{k_{z,m}}{\omega\mu} \\ \frac{\omega\varepsilon}{k_{z,m}} & 0 & -\frac{\omega\varepsilon}{k_{z,m}} & 0 \end{pmatrix} \begin{pmatrix} T_{xm} \\ T_{ym} \\ R_{xm} \\ R_{ym} \end{pmatrix}, \quad \text{(A.21)}$$

omitting the z-dependence. One may also write it in terms of block matrices, that is, writing k_z for the diagonal matrix with the numbers $k_{z,m}$ on the diagonal:

$$C = \begin{pmatrix} 0 & -\frac{k_z}{\omega\mu} \\ \frac{\omega\varepsilon}{k_z} & 0 \end{pmatrix}. \quad \text{(A.22)}$$

With this notation, equation (A.21) becomes

$$F = \begin{pmatrix} [E_x] \\ [E_y] \\ [H_x] \\ [H_y] \end{pmatrix} = \begin{pmatrix} 1 & 0 & 1 & 0 \\ 0 & 1 & 0 & 1 \\ 0 & -\frac{k_z}{\omega\mu} & 0 & \frac{k_z}{\omega\mu} \\ \frac{\omega\varepsilon}{k_z} & 0 & -\frac{\omega\varepsilon}{k_z} & 0 \end{pmatrix} \begin{pmatrix} [T_x] \\ [T_y] \\ [R_x] \\ [R_y] \end{pmatrix} = \begin{pmatrix} 1 & 1 \\ C & -C \end{pmatrix} \begin{pmatrix} T \\ R \end{pmatrix} =: QS. \quad \text{(A.23)}$$

So, the propagation vector S can be translated into the corresponding field vector by a simple matrix multiplication with Q. If Q is invertible, the way back, from field vector to propagation vector,

$$S = Q^{-1}F, \quad \text{(A.24)}$$

works too. But is Q invertible? If its determinant is non-zero, it is invertible. So, let us have a look at the determinant. According to [70, 71] the determinant of a 2x2-block matrix

$$\det \begin{pmatrix} Q_{11} & Q_{12} \\ Q_{21} & Q_{22} \end{pmatrix} = \det \left(Q_{11}Q_{22} - Q_{12}Q_{21}\right), \quad \text{(A.25)}$$

if $Q_{21}Q_{22} = Q_{22}Q_{21}$. So, the determinant of the conversion matrix

$$\det(Q) = \det\left(2\begin{pmatrix} 0 & -\frac{k_z}{\omega\mu} \\ \frac{\omega\varepsilon}{k_z} & 0 \end{pmatrix}\right) = 2^{2(2N+1)} \det\begin{pmatrix} 0 & -\frac{k_z}{\omega\mu} \\ \frac{\omega\varepsilon}{k_z} & 0 \end{pmatrix} \tag{A.26}$$

$$= -2^{2(2N+1)} \left(\Pi_{m=-N}^{N} \frac{\omega\varepsilon}{k_{z,m}}\right)\left(\Pi_{m=-N}^{N} \frac{-k_{z,m}}{\omega\mu}\right) \neq 0, \tag{A.27}$$

if $k_{z,m} \neq 0 \; \forall \; m \in \{-N, \; -N+1, \; \cdots, N\}$. An unfortunate choice of d or λ can lead to $k_{z,m} = 0$ for some m. But in this case, the conversion matrix itself is not defined because it contains $1/k_{z,m}$-entries.

Bibliography

[1] Jerzy Plebanski. "Electromagnetic Waves in Gravitational Fields". In: *Phys. Rev.* 118.5 (1959), pp. 1396–1408.

[2] U. Leonhardt and T. G. Philbin. "Transformation Optics and the Geometry of Light". In: *ArXiv e-prints* (May 2008). arXiv: 0805.4778 [physics.optics].

[3] D. Schurig, J. B. Pendry, and D. R. Smith. "Calculation of material properties and ray tracing in transformation media". In: *Optics Express* 14 (Oct. 2006), pp. 9794–9804. DOI: 10.1364/OE.14.009794. eprint: physics/0607205.

[4] N. B. Kundtz, D. R. Smith, and J. B. Pendry. "Electromagnetic Design With Transformation Optics". In: *Proceedings of the IEEE* 99.10 (2011), pp. 1622–1633. ISSN: 0018-9219. DOI: 10.1109/JPROC.2010.2089664.

[5] Edward J. Rothwell and Michael J. Cloud. *Electromagnetics*. CRC Press LLC, 2001.

[6] Walter Greiner. *Classical electrodynamics*. Springer-Verlag New-York, Inc., 1998.

[7] L. D. Landau and E. M. Lifshitz. *The Classical Theory of Fields*. Vol. 4. Butterworth Heinemann, 1994.

[8] L. D. Landau, E. M. Lifshitz, and L. P. Pitaevskii. *Electromagnetics of Continuous Media*. Pergamon Press, 1984.

[9] John David Jackson. *Classical Electrodynamics*. John Wiley & Sons, Inc., 1999.

[10] David J. Griffiths. *Introduction To Electrodynamics (1989)*. Prentice-Hall, Inc.

[11] Robert D. Guenther. *Modern Optics*. John Wiley & Sons Inc., New York, 1990.

[12] U. Leonhardt and T. G. Philbin. "General relativity in electrical engineering". In: *New Journal of Physics* 8 (Oct. 2006), p. 247. DOI: 10.1088/1367-2630/8/10/247. eprint: cond-mat/0607418.

[13] D. S. Kulyabov, A. V. Korolkova, and L. A. Sevastyanov. "The simplest geometrization of Maxwell's equations". In: *ArXiv e-prints* (Feb. 2014). arXiv: 1402.5527 [math-ph].

[14] A. J. Ward and John B. Pendry. "Refraction and geometry in Maxwell's equations". In: *Journal of modern optics* 43.4 (1996), pp. 773–793.

[15] J. Chandezon, D. Maystre, and G. Raoult. "A new theoretical method for diffraction gratings and its numerical application". In: *J. Optics (Paris)* 11.4 (1980), pp. 235–241.

[16] Gérard Granet. "Coordinate Transformation Methods". In: *Gratings: Theory and Numerical Applications*. Ed. by Evgeny Popov. Aix Marseille Université, CNRS, Centrale Marseille, Institut Fresnel UMR 7249: Presses Universitaires de Provence, 2014. Chap. 8, pp. 309–340. URL: http://www.fresnel.fr/numerical-grating-book-2.

[17] D. Schurig, J. B. Pendry, and D. R. Smith. "Transformation-designed optical elements". In: *Optics Express* 15.22 (2007), pp. 14772–14782.

[18] J. B. Pendry, D. Schurig, and D. R. Smith. "Controlling Electromagnetic Fields". In: *Science* 312 (June 2006), pp. 1780–1782. DOI: 10.1126/science.1125907.

[19] D. Schurig et al. "Metamaterial Electromagnetic Cloak at Microwave Frequencies". In: *Science* 314 (Nov. 2006), pp. 977–980. DOI: 10.1126/science.1133628.

[20] Raymond Rumpf. "Design and optimization of nano-optical elements by coupling fabrication to optical behavior". PhD thesis. University of Central Florida, Orlando, Florida.

[21] Cesar R. Garcia et al. "3D printing of anisotropic metamaterials". In: *Progress In Electromagnetics Research Letters* 34 (2012), pp. 75–82.

[22] Jason Valentine et al. "Three-dimensional optical metamaterial with a negative refractive index". In: *nature* 455.7211 (2008), pp. 376–379.

[23] Maximilian Auer. "Numerische Analyse optischer Nanostrukturen mit dreidimensionalen rigorosen Methoden ". MA thesis. Universität Heidelberg, Institut für Technische Informatik, Lehrstuhl für Optoelektronik, 2009.

[24] Steven A. Cummer et al. "Full-wave simulations of electromagnetic cloaking structures". In: *Physical Review E* 74.3 (2006), p. 036621.

[25] S. A. Cummer, R. Liu, and T. J. Cui. "A rigorous and nonsingular two dimensional cloaking coordinate transformation". In: *Journal of Applied Physics* 105.5, 056102-056102-3 (Mar. 2009), pp. 056102–056102–3. DOI: 10.1063/1.3080155.

[26] W. Cai et al. "Optical cloaking with metamaterials". In: *Nature Photonics* 1 (Apr. 2007), pp. 224–227. DOI: 10.1038/nphoton.2007.28. eprint: physics/0611242.

[27] Robert T. Thompson, Steven A. Cummer, and Jörg Frauendiener. "Generalized transformation optics of linear materials". In: *Journal of Optics* 13.5 (2011), p. 055105.

[28] Robert T. Thompson, Steven A. Cummer, and Jörg Frauendiener. "A completely covariant approach to transformation optics". In: *Journal of Optics* 13.2 (2010), p. 024008.

[29] Robert T. Thompson. "Transformation optics in nonvacuum initial dielectric media". In: *Physical Review A* 82.5 (2010), p. 053801.

[30] Koki Watanabe, Roger Petit, and Michel Nevière. "Differential theory of gratings made of anisotropic materials". In: *J. Opt. Soc. Am. A* 19.2 (2002), pp. 325–334. DOI: 10.1364/JOSAA.19.000325. URL: http://josaa.osa.org/abstract.cfm?URI=josaa-19-2-325.

[31] Evgeny Popov and Michel Nevière. "Maxwell equations in Fourier space: fast-converging formulation for diffraction by arbitrary shaped, periodic, anisotropic media". In: *JOSA A* 18.11 (2001), pp. 2886–2894.

[32] Evgeny Popov. "Differential Method for Periodic Structures". In: *Gratings: Theory and Numerical Applications*. Ed. by Evgeny Popov. Aix Marseille Université, CNRS, Centrale Marseille, Institut Fresnel UMR 7249: Presses Universitaires de Provence, 2014. Chap. 7, pp. 251–307. URL: http://www.fresnel.fr/numerical-grating-book-2.

[33] L. Li. "Fourier modal method for crossed anisotropic gratings with arbitrary permittivity and permeability tensors". In: *Journal of Optics A: Pure and Applied Optics* 5 (July 2003), pp. 345–355. DOI: 10.1088/1464-4258/5/4/307.

[34] R. Petit. "Electromagnetic Theory of Gratings". In: *Electromagnetic Theory of Gratings. Series: Topics in Current Physics* 22 (1980). DOI: 10.1007/978-3-642-81500-3.

[35] Gérard Tayeb. “Contribution à l’étude de la diffraction des ondes électro–magnétiques par des réseaux. Réflexions sur les méthodes existantes et sur leur extension aux milieux anisotropes”. PhD thesis. Université Paul Cézanne - Aix-Marseille III, 1990. URL: "https://tel.archives-ouvertes.fr/tel-00323714".

[36] Maximilian Auer. “Numerical treatment of localized fields in rigorous diffraction theory and its application to light absorption in structured layers”. PhD thesis. University Heidelberg, Combined Faculty for the Natural Sciences and Mathematics, 2016.

[37] M. G. Moharam et al. “Stable implementation of the rigorous coupled-wave analysis for surface-relief gratings: enhanced transmittance matrix approach”. In: *Journal of the Optical Society of America A* 12 (May 1995), pp. 1077–1086. DOI: 10.1364/JOSAA.12.001077.

[38] Hans Rudolf Schwarz and Norbert Köckler. *Numerische Mathematik*. Vieweg+Teubner Verlag, 2001.

[39] W. Press et al. *Numerical Recipes. The Art of Scientific Computing*. Vol. 3. 2007.

[40] Karl Strehmel, Rüdiger Weiner, and Helmut Podhaisky. *Numerik gewöhnlicher Differentialgleichungen. Nichtsteife, steife und differentialalgebraische Gleichungen*. Vieweg+Teubner Verlag, 2012.

[41] Koki Watanabe. “Fast converging and widely applicable formulation of the differential theory for anisotropic gratings”. In: *Progress In Electromagnetics Research* 48 (2004), pp. 279–299.

[42] Koki Watanabe. “Study of the differential theory of lamellar gratings made of highly conducting materials”. In: *JOSA A* 23.1 (2006), pp. 69–72.

[43] Evgeni Popov and Michel Nevière. “Grating theory: new equations in Fourier space leading to fast converging results for TM polarization”. In: *JOSA A* 17.10 (2000), pp. 1773–1784.

[44] Eng Leong Tan. “Note on formulation of the enhanced scattering-(transmittance-) matrix approach”. In: *JOSA A* 19.6 (2002), pp. 1157–1161.

[45] L. Li. “Formulation and comparison of two recursive matrix algorithms for modeling layered diffraction gratings”. In: *JOSA A* 13.5 (1996), pp. 1024–1035.

[46] N. P. K. Cotter, T. W. Preist, and J. R. Sambles. "Scattering-matrix approach to multilayer diffraction". In: *JOSA A* 12.5 (1995), pp. 1097–1103.

[47] F. Montiel and M Neviere. "Differential theory of gratings: extension to deep gratings of arbitrary profile and permittivity through the R-matrix propagation algorithm". In: *JOSA A* 11.12 (1994), pp. 3241–3250.

[48] Walter Zulehner. *Numerische Mathematik: Eine Einführung anhand von Differentialgleichungsproblemen Band 2: Instationäre Probleme*. Springer Basel AG, 2011.

[49] Michael Ernst Geiger. "Adaptive Multiple Shooting for Boundary Value Problems and Constrained Parabolic Optimization Problems". PhD thesis. Ruprecht-Karls Universität Heidelberg, 2015. URL: "http://nbn-resolving.de/urn:nbn:de:bsz:16-heidok-187746".

[50] L. Li. "Multilayer modal method for diffraction gratings of arbitrary profile, depth, and permittivity". In: *JOSA A* 10.12 (1993), pp. 2581–2591.

[51] F. Montiel, M. Neviere, and P. Peyrot. "Waveguide confinement of Cerenkov second-harmonic generation through a graded-index grating coupler: electromagnetic optimization". In: *Journal of Modern Optics* 45 (Oct. 1998), pp. 2169–2186. DOI: 10.1080/09500349808231753.

[52] Koki Watanabe. "Numerical integration schemes used on the differential theory for anisotropic gratings". In: *J. Opt. Soc. Am. A* 19.11 (2002), pp. 2245–2252. DOI: 10.1364/JOSAA.19.002245. URL: http://josaa.osa.org/abstract.cfm?URI=josaa-19-11-2245.

[53] Raymond C Rumpf. "Improved formulation of scattering matrices for semi-analytical methods that is consistent with convention". In: *Progress In Electromagnetics Research B* 35 (2011), pp. 241–261.

[54] Martin Hanke-Bourgeois. *Grundlagen der numerischen Mathematik und des wissenschaftlichen Rechnens*. Vol. 3. Springer, 2009.

[55] Peter Knabner and Wolf Barth. *Lineare Algebra*. Springer, 2013.

[56] Stephen J. Wright. "Stable parallel algorithms for two-point boundary value problems". In: *SIAM Journal on Scientific and Statistical Computing* 13.3 (1992), pp. 742–764.

[57] Pierluigi Amodio et al. "Almost block diagonal linear systems: sequential and parallel solution techniques, and applications". In: *Numerical linear algebra with applications* 7.5 (2000), pp. 275–317.

[58] Pochi Yeh. "Optics of anisotropic layered media: a new 4× 4 matrix algebra". In: *Surface Science* 96.1-3 (1980), pp. 41–53.

[59] Åke Björck. *Numerical methods in matrix computations*. Springer, 2015.

[60] D. A. Roberts, N. Kundtz, and D. R. Smith. "Optical lens compression via transformation optics". In: *Optics Express* 17 (Sept. 2009), p. 16535. DOI: 10.1364/OE.17.016535.

[61] K.-H. Brenner. *Computational Optics*. Skript zur Vorlesung. 2014.

[62] Maximilian Auer and Karl-Heinz Brenner. "Localized input fields in rigorous coupled-wave analysis". In: *JOSA A* 31.11 (2014), pp. 2385–2393.

[63] The Mathworks Inc. *MATLAB version R2017b*. Natick, Massachusetts, 2017.

[64] Marco Rahm et al. "Optical design of reflectionless complex media by finite embedded coordinate transformations". In: *Physical Review Letters* 100.6 (2008), p. 063903.

[65] Martin Schmiele et al. "Designing optical elements from isotropic materials by using transformation optics". In: *Physical Review A* 81.3 (2010), p. 033837.

[66] Mark Galassi et al. *GNU Scientific Library Reference Manual (Network Theory Ltd., 2009)*. 3rd ed. 2009. ISBN: 0954612078.

[67] E. Anderson et al. *LAPACK Users' Guide*. Third. Philadelphia, PA: Society for Industrial and Applied Mathematics, 1999. ISBN: 0-89871-447-8 (paperback).

[68] Joseph W. Goodman. *Introduction to Fourier Optics*. The McGraw-Hill Companies, Inc.

[69] Evgeny Popov et al. "Staircase approximation validity for arbitrary-shaped gratings". In: *JOSA A* 19.1 (2002), pp. 33–42.

[70] John R. Silvester. "Determinants of Block Matrices". In: *The Mathematical Gazette* 84.501 (2000), pp. 460–467. ISSN: 00255572. URL: http://www.jstor.org/stable/3620776.

[71] Nat Sothanaphan. "Determinants of block matrices with noncommuting blocks". In: *Linear Algebra and its Applications* 512 (2017). DOI: 10.1016/j.laa.2016.10.004.

Danksagung:

An dieser Stelle möchte ich mich bei all denjenigen bedanken, die mich während der Anfertigung dieser Masterarbeit unterstützt haben.

Zunächst gebührt mein Dank Prof. Dr. Karl-Heinz Brenner für die Möglichkeit, diese Arbeit am Lehrstuhl für Optoelektronik anzufertigen. Für die hilfreiche Unterstützung in jedweden wissenschaftlichen Fragen sowie die konstruktiven Anregungen bei der Erstellung dieser Arbeit möchte ich mich herzlich bedanken.

Ein weiterer Dank gilt André Junker und Tim Stenau für ihre stetige Hilfsbereitschaft.

Zuletzt möchte ich Sabine Volk und Wolfgang Stumpfs für ihre Unterstützung in allen praktischen und organisatorischen Belangen danken.

Erklärung:

Ich versichere, dass ich diese Arbeit selbstständig verfasst habe und keine anderen als die angegebenen Quellen und Hilfsmittel benutzt habe.

Heidelberg, den (Datum) .....